PEOPLE'S DEMOCRATIC REPUBLIC OF ALGERIA

MINISTRY OF HIGHER EDUCATION AND SCIENTIFIC RESEARCH

MOHAMED BOUDIAF UNIVERSITY - M'SILA

FACULTY OF TECHNOLOGY

DEPARTMENT OF ELECTRONICS

Thesis presented for obtaining

Academic Master's degree

By:

BOUGUERRA Yaaqoub

ZOUAOUI Faiz

THEME

Design and Analysis of High Performance 2D Photonic Crystal Based Sensors for Biomedical Sensing Applications

Defended before the jury composed of:

Pr. HOCINI Abdesselam	President	Univ. M'sila
Dr. HARHOUZ Ahlam	Supervisor	Univ. M'sila
Dr. TAYOUB Hadjira	Co-Supervisor	URMM/CRTI.Annaba
Dr. ZOUACHE Tarek	Examiner	Univ. M'sila
Dr. Salah KHENNOUF	Examiner	Univ. M'sila

Year: 2023/2024

THANKING

First of all, we want to thank Allah, the Almighty, for giving us so much courage, patience, and will to achieve this goal.

We would like to thank our supervisors

Dr. Harhouz Ahlam (Senior lecturer A at the University of M'sila)

Dr. Tayoub Hadjira (Senior researcher A at URMM/CRTI)

All our thanks also go to the members of the jury for having given us the honor to judge this modest work.

Our thanks also go to all the people who have helped us and supported us from near or far in the realization of this work.

DEDICATION

In the name of Allah, the Most Merciful, the Merciful.

First of all, I would like to thank the Almighty for giving me the courage and patience to get to this stage in order to accomplish this work to which I dedicate:

To my dear mother: who never ceased to pray for me

To my dear father for his encouragement

To my dear brothers

To my whole big family

To best friends

To all my friends at Msila University

Bouguerra Yaaqoub

I dedicate this humble work to my father, who hasn't given me so little time, and...

Big for my mom who's been with me my whole study career.

To all my brothers, to all those who extend my family.

To my friend and comrade.

To everyone who taught me a letter all the way to school.

To this day.

To everyone who taught me patience in a difficult direction.

To both of you, light to the path of success.

And many of my friends.

Dean, help me with this.The trip.

Zouaoui Faiz

Table of Contents

Chapter III design and simulation of 2D photonic crystals sensors for bio-detections

List of figures

LIST OF TABLES

LIST OF ABBREVIATIONS

Abbreviation	Explanation
PhC or PC	Photonic Crystal
PBG	Photonic bandgap
2D	Two-Dimensional
FDTD	Finite-Difference Time-Domain
PML	Perfectly Matched Layer
PCW	Photonic Crystal Waveguide
RI	Refractive Index
SPR Surface	Plasmon Resonance
TE	Transverse Electric
TM	Transverse Magnetic

Introduction general

Introduction general

In recent years, many technological advances in human history have come from our understanding of materials and our ability to design unique and desirable material properties for a number of applications. From our prehistoric ancestors, who built durable stone and iron tools, to the first semiconductor device engineers, who learned to precisely control the conductivity of a material, our ability to design and manufacture useful structures is based on the growing collection of natural and artificial materials. During the last century, we have seen how the adaptation of the electrical properties of a semiconductor has enabled the invention and demonstration of many devices, which has triggered an information technology revolution that continues to transform the computing, data storage, and communication capabilities of our society [1]. Recent advances in micro-technologies including the reduction of physical characteristics and the miniaturization of devices, have now made it possible to manufacture denser and faster electronic circuits. However, many challenges arise as we continue to reduce the dimensions of the devices further. In particular, due to high energy consumption and electromagnetic interference (EMI), metal interconnections pose a fundamental problem for the next generation of electronic circuits [2].

In this context, photonic crystals (PhCs) proposed by Yablonovitch, in 1987 [3] and S. John [4] in adhesive articles could play an important role. These PhCs are actually the analogue of a semiconductor that controls photons [5], they are periodic artificial structures whose dielectric index periodically changes in one or more spatial directions at a wavelength scale that we want to control [6].

Photonic crystal structures (PhCs) are formed by stacking materials whose refractive index varies periodically in one, two, or three dimensions [Reference]. This periodicity of the medium induces the light spreading in this crystal; an effect similar to that of the periodic potential on the electrons in a crystal. Just as there are permissible energy bands and prohibited bands for electrons; there are photonic bands of permissive states and forbidden bands [3]. A photonic band corresponds to a mode that spreads in the photonic crystal, and a photonic band gap (PBG) corresponds to an energy interval where the spread of light is prohibited in certain directions of that crystal [4].

The potential applications of 2D photon banned bands (PBGs) are diverse and multiple. Among other things, we find the realization of resonant cavities of very small size, waveguides, curves, selective filters, multipliers – demultiplexers, and optical fibers. These materials have produced new optoelectronic components that are more efficient and more compact than the conventional components currently known [5].

The last two decades have seen a very remarkable union of biology and photonics. The promises of bio-photonics are immense. This field is at the interface between optics, chemistry, life sciences, and medicine. The simple, quick, and efficient detection of chemical or biological molecules has become an important challenge for the health, environment, agriculture, and agro-food sectors [6]. Of the current biosensors, those that operate optical detection have the highest sensitivity. The principle of operation of passive optical sensors is based on the variations in their optical properties when the refractive index (RI) of the analyzer changes.

Part of the Covid-19 for patent. Everything related to this aspect is available in the patent file under number N° :240457.

The work of this master thesis is part of this perspective, while exploiting a new approach that allows the design and study of refraction index (RI) sensors based on two-dimensional PhCs operating in the visible medium. The structures proposed in this work are essentially based on a guide-cavity coupling system. We have set ourselves the goal of strengthening the confinement of light within the cavity. In the present work, an ultra-compact 2D-PhC bio-sensor is designed, and good sensing characteristics such as sensitivity, Q-factor, FOM, detection limit, resonant wavelength, and normalized transmission are estimated for the normal and abnormal brain tissues for the proposed biosensor. The proposed high-performance PhC biosensor can be used as a powerful tool to accurately distinguish between normal and abnormal brain tissues, it has a simple structure, an ultra-compact size, and high confinement of light within the microcavity region. All the simulations are done using Plane Wave Expansion (PWE) method and Finite- Difference Time-Domain (FDTD) tool of RSoft Photonic Suite CAD.

In order to present most of our work, we will give the master thesis the following structure:

The first chapter is devoted to an introduction to photonic crystals. We will begin by introducing photonic crystals and presenting their general notions. After a brief recall of the

different types of photon crystals, we will focus our study on two-dimensional photon crystals (2D-PhC).

Then, in the second chapter, the development and investigation of optical biosensors will be investigated, where a range of biosensors for the detection of different biological samples will be reviewed. This chapter focuses on the study of RI biosensors based on photonic crystals.

Finally, in the last chapter, the design of cavity sensors coupled with a guide based on PhCs that can be used for (RI) detection, where the detection of an analytic can be performed by changing (RI). We will also study the effect of physical and geometric parameters on the performance of the proposed sensors in order to improve their performance. All simulations will be performed using both the (PWE) and (FDTD) methods of the FullWAVE and BandSOLVE simulator from RSoft Photonic Suite CAD. We will conclude this master thesis with a general conclusion summarizing the results achieved, thus proposing some perspectives.

.

Chapter 1

Photonic crystals: from theory to practice

I-1 Introduction

Photonic crystals (PhCs) are very promising systems for applications in the field of electromagnetic waves, with real achievements in the areas of microwaves, optoelectronics and optical telecommunications, and the medical field. In this chapter, we will present the basic design of photonic crystals. For this, their characteristics, the principle of the photonic band gap, and the band diagram will be explained. We will then give an overview of the different types of PhCs and their main applications**.**

I-2 Historical

Advances in nanotechnology have made it possible to develop artificial materials whose behavior in relation to electromagnetic waves is quite surprising, and, for this reason, they are sometimes called photonic crystals. Since then, these materials have been of great interest to the scientific community, especially in the field of optics. The term "photonic crystal" was first used more than 100 years ago, with the first assumptions about the possibility of controlling the propagation of light using periodic structures dating back to 1887 with the work of Lord Rayleigh. The field of photonic crystals began in 1987, when Eli Yabonovitch and Saier John introduced the concept of banned material separately and in different contexts [3].

In 1991, A. Genack *et al*. [7] experimentally demonstrated the existence of the light localization effect in periodic structures. At the same time, Yablonovitch had demonstrated the first banned 3D photonic strip in the microwave region. In 1993, Yablonovitch [8] designed the first three-dimensional photonic crystal with a band banned in the microwave. This photonic crystal is named after its inventor, "Yablonovite.". In 1996, Thomas Krauss demonstrated the first 2D photonic crystal with an optical wavelength [9]. In 2000, the first three-dimensional photonic crystal with a full photonic band gap in the near-infrared domain was obtained [10]. In recent years, research in the field of photonic crystals has experienced extraordinary expansion and has covered almost all scientific disciplines, making unprecedented progress.

I-3 Definition of photonic crystals

Semiconductors are very interesting materials from the point of view of information control, as they form the basics of electronic circuits (transistors, diodes, and electrical components). The banned electronic band delimits a controllable excitation channel for electrons, since the bonds between atoms are ensured for all available electrons. To ensure conductivity, it is necessary to release the electrons by providing enough energy to break a bond

and move from the valence band to the semiconductor's conductive band. This energy that separates these two bands defines an electronic banned band [12;14].

Photonic crystals (PhCs) or banned band materials are structures whose dielectric index periodically varies on the wavelength scale in one or more directions of space because they produce a certain frequency region where the propagation of electromagnetic waves is prohibited, what is called the banned photonic band (*PBG*) [15]. This interesting priority offers photonic crystals the possibility of controlling the spread of electromagnetic waves without absorption and thus enables new perspectives for the manipulation of light. Photonic crystals are structures whose dielectric index varies periodically on the scale of the wavelength to be controlled in one or more directions of space [16]. This periodic variation of the optical index in different directions leads to the appearance of frequency ranges in which light can no longer spread. In nature, some animal and mineral species have used and manufactured these structures for aesthetic and strategic purposes for a long time (**Figure I.1**) and it is recently that humans have found applications there [15].

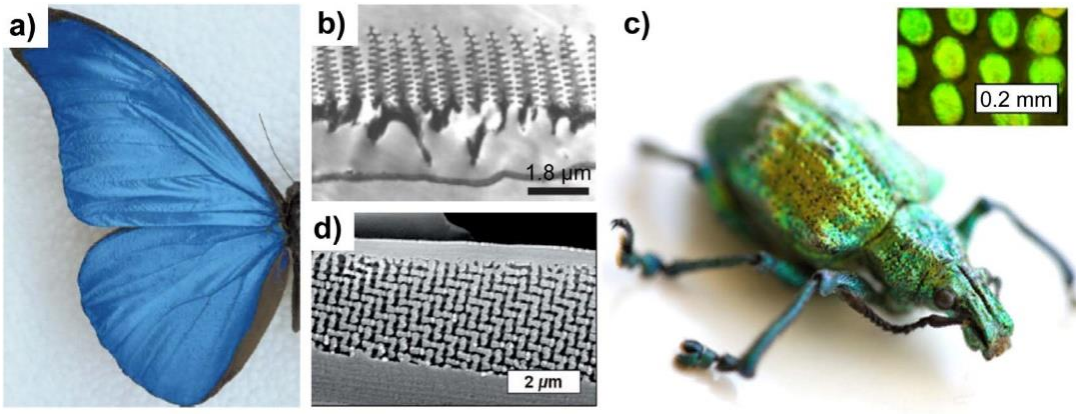

Figure I.1: Examples of natural photonic crystal [13].

I-4 Photonic crystal's structure

In a semiconductor, the periodic variation in the potential of interaction between electrons and atoms causes the electrons to have access only to certain levels of energy, permissible energy bands, separated by banned bands of energy. This concept of permitted and prohibited bands can be extended to the behavior of photonics in a photonic crystal. Because of the periodic variation in the refractive index in a photonic crystal, the energy of the photonics is quantified in permitted and prohibited bands, also called gaps [17].

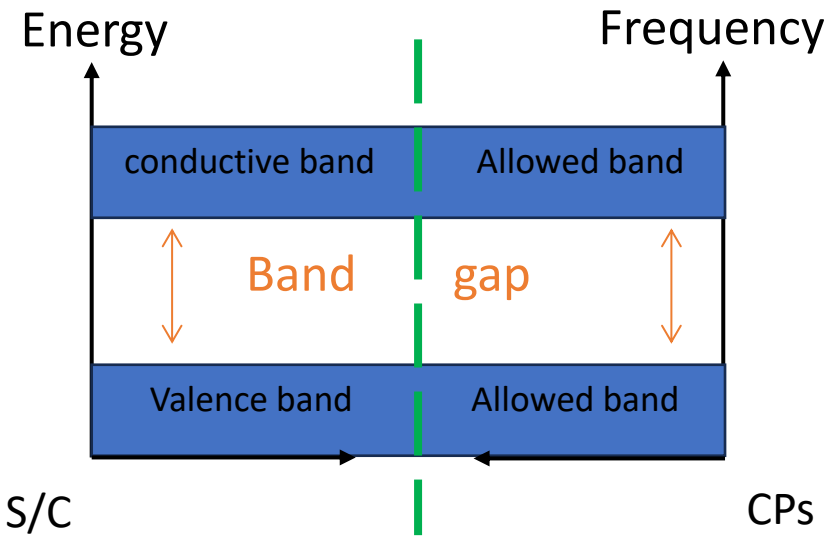

Figure I.2: Structure of semiconductor and PhCs.

A photonic band gap of a crystal is called complete (or total) when, for the frequency range in question, the crystal does not support any electromagnetic mode of propagation; that is, a wave whose frequency is within the total banned range cannot propagate in the crystal no matter its polarization or its propagation direction [17].

Experimentally, a banned band is identified by measuring the response of the material exposed to a light beam, in transmission or in reflection. The latter is characterized by the appearance of a minimum of transmission and, therefore, a maximum of reflection.

I-5 Characteristics of photonic crystals

I-5-1 Dimensionality (Classifications of photonic crystal)

It is determined by the periodicity of the refraction index. The periodicity of a photonic crystal can extend to one, two, or three dimensions. The number of directions of the refraction index (RI) periodicity indicates the type of photonic crystal:

- **Periodicity in one direction:** 1D photonic crystal or Bragg mirror.
- **Periodicity in two directions of space:** 2D photonic crystal.
- **Periodicity in all directions in space:** 3D photonic crystal.

The schematic representations of the PhCs structures are presented in the following figure (**Figure I.3)**:

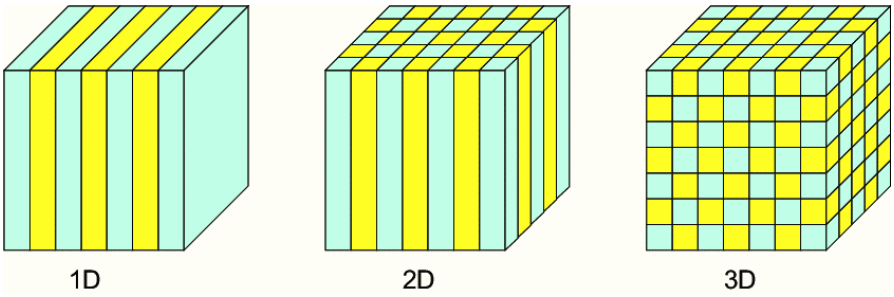

Figure I.3: Examples of classifications of photonic crystal [15].

I-5-2 Defects in a photonic crystal

As with semiconductors, where energy levels appear in the gap when inserting impurities (atoms other than those of the crystal), extrinsic defects within CP create permissible energy levels, called "defect modes," for particular frequencies in the forbidden band [19]. Defects in photonic crystals refer to irregularities or intentional modifications in the periodic structure of the crystal lattice that disrupt the perfect periodicity of the crystal. These defects can significantly impact the photonic properties and behavior of light within the crystal. There are different types of defects in photonic crystals, and they serve various purposes in designing photonic devices and systems. Here are some common types of defects in photonic crystals:

A- Point defects: They are created by changing the characteristics of a cell in the network. For two-dimensional photonic crystals, the point defect can be obtained by changing the permittivity, size, or shape of patterns. We will simply mention the three most frequently performed types of point defects [12]:

- **Additive defects:** They consist of the addition of additional elements to the original periodic network. This type of defect has two types [20].

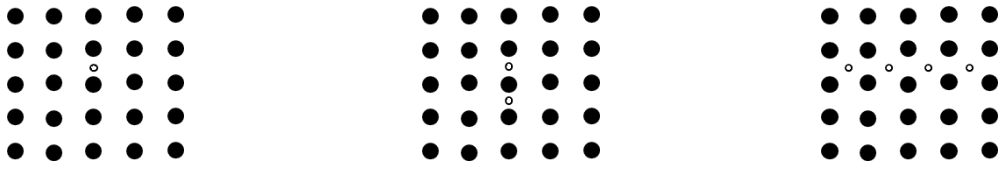

Figure I.4: Different additive defect strategies [12]**.**

- **Lacunar defects**: Unlike additive defects, where elements of the original periodic network are removed. In Figure I.5, we show the different strategies for lacuna defects.

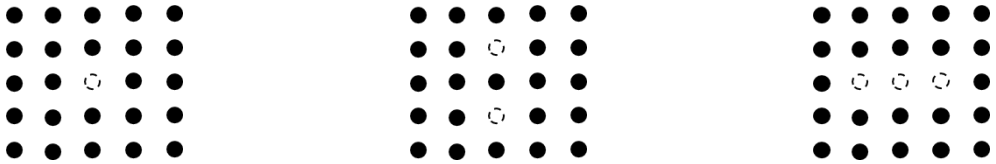

Figure I.5: Different gaps strategies [16].

- **Replacement defects**: Consist of changing elements of the original network, either the diameter or the permissiveness of certain patterns.

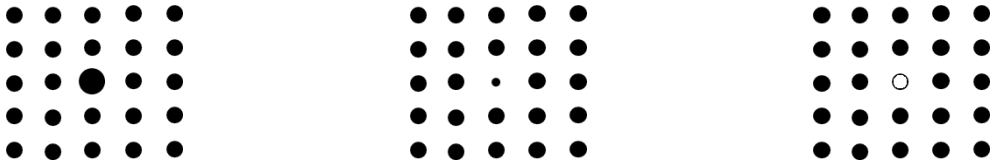

Figure I.6: Different types of replacement defects [16].

B- Linear defects: A linear defect in photonic crystals is a row of patterns removed or modified in one or more directions of the original crystal's periodicity. This type of fault is called a waveguide. These linear defects are very interesting for rectilinear waveguides, types [21]:

- **Vacancies:** Vacancies occur when one or more lattice sites within the photonic crystal lattice are intentionally left unoccupied. They create localized regions where there is no photonic crystal material. Vacations can have the following effects:
  - Create defect modes within the photonic bandgap.
  - Modify the density of photonic states.
  - Influence the dispersion relations of guided modes.
  - Enable the design of defect-mode microcavities and resonators.

- **Interstitials:** Intentionally adding extra lattice sites or constituents to the photonic crystal lattice is known as introducing interstitial defects. Interstitials can trap and scatter photonics, affecting the crystal's optical properties.
- **Substitutional defects:** Substitutional defects involve replacing one type of constituent material in the photonic crystal lattice with another type at specific lattice sites. Substitutional defects can:
  - Modify the local refractive index, leading to controlled light manipulation.
  - Create localized defect modes.
  - Be used to engineer heterostructures within the photonic crystal [22].

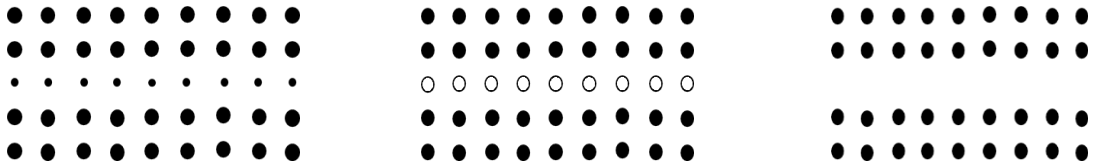

Figure I.7: Different types of linear defects: (a) Dimensions of elementary patterns, (b) Permissibility of elementary patterns; (c) Vacuum defect [22].

C- **Coupled defects:** In the context of photonic crystals, it refers to coupled defects within a photonic crystal lattice. In photonic crystals, defects are intentional modifications or irregularities in the periodic structure of the crystal that are introduced to tailor the behavior of light within the crystal. When multiple defects are present and interact with each other, they can give rise to interesting and potentially useful optical phenomena. Here's an overview of "default couples" or coupled defects in photonic crystals [23]:

- **Coupled Resonators**: One common example of coupled defects in photonic crystals involves creating multiple microcavities or resonators within the crystal lattice. These resonators can be designed to interact with each other through evanescent fields, resulting in coupled resonator effects.
- **Mode Splitting**: When two or more microcavities are close enough to interact, their resonant modes can split into new eigenmodes due to the coupling between them. This can lead to the creation of new spectral features in the transmission or reflection spectrum of the photonic crystal.
- **Enhanced Light-Matter Interaction:** Coupled defects can enhance the interaction between light and matter (e.g., quantum dots or molecules) placed within the cavities. This is useful for applications like efficient single-photonic sources.

D- **Waveguide-Cavity Coupling:** Another form of coupled defect involves coupling a waveguide defect (a defect acting as a waveguide) with a cavity defect. This can lead to various interesting phenomena:

- **Waveguide-Cavity Mode Matching:** By carefully designing the coupling between the waveguide and cavity, it's possible to achieve efficient mode matching, allowing light from the waveguide to be efficiently coupled into the cavity.
- **Resonance Tuning** Coupled defects can be used to tune the resonance frequency of the cavity by adjusting the coupling strength between the waveguide and the cavity.

E- **Defect Arrays:** Arrays of defects in a photonic crystal can also exhibit coupled defect effects. When defects are arranged in a specific pattern or geometry, they can interact with each other in a collective manner.

- **Band edge Modes:** In periodic arrays of coupled defects, photonic bandgap modes can emerge at specific frequencies within the bandgap, forming band-edge modes. These modes are influenced by the collective behavior of the coupled defects.
- **Fano Resonances** Coupled defect arrays can exhibit Fano resonances, which are asymmetric spectral features that arise due to the interference between discrete defect modes and the background photonic crystal modes.

Coupled defects in photonic crystals are extensively studied and engineered to create novel optical devices and systems with tailored spectral properties, enhanced light-matter interactions, and advanced functionalities. Researchers use these coupled defect structures for various applications, including filters, sensors, lasers, and quantum information processing devices.

I-5-3 Symmetry

Symmetry plays a crucial role in the design, analysis, and understanding of photonic crystals. Photonic crystals are periodic dielectric structures that exhibit unique optical properties due to their structural symmetry [24]. Here are some important aspects of symmetry in photonic crystals:

- **Crystal symmetry:** Photonic crystals are typically composed of dielectric materials arranged in a periodic lattice structure. The type of crystal lattice and its symmetry operations define the crystal's overall symmetry. Common crystal structures for photonic crystals include simple cubic, face-centered cubic, hexagonal, and others.
- **Symmetry operations:** Symmetry operations in photonic crystals include translations, rotations, reflections, and inversions. These operations are used to map one part of the crystal onto another while preserving its structural characteristics. The combination of these operations defines the crystal's point-group symmetry.
- **Reciprocal space symmetry:** In the context of photonic crystals, the reciprocal lattice plays a crucial role in analyzing their optical properties. The reciprocal lattice is also subject to symmetry operations, and the symmetry of the reciprocal lattice is related to the symmetry of the direct (real-space) lattice.
- **Symmetry-Protected Modes:** Certain photonic crystal modes are protected by symmetry and are robust against disorder or structural imperfections. These modes are

of particular interest in applications where high-quality optical resonators or waveguides are required.

I-5-4 Topology

The topology reflects the architecture and the compactness of the material. A network of a given symmetry may present different topologies (cases of interpenetrated, in contact, or isolated constituent bricks) [25]. Topological properties of their band structures and photonic modes. Here are some characteristic features of topological properties in photonic crystals:

- **Topological Bandgaps:** Topological photonic crystals can exhibit bandgaps in their optical spectra. These bandgaps are topologically non-trivial and often associated with specific symmetry-protected topological properties:
- **Edge or Surface States:** A key characteristic of topological photonic crystals is the presence of topologically protected edge or surface states within the bandgap. These states are robust against defects or structural imperfections and are typically associated with non-trivial topological invariants.
- **Topological Invariants**: Topological invariants, such as Chern numbers, topological indices, or winding numbers, are used to quantify the topological properties of photonic band structures. These invariants provide information about the nature and stability of topological states.
- **Protection against Backscattering:** Topologically protected photonic modes are less susceptible to scattering and backscattering, making them highly desirable for various applications, including optical communication and quantum information processing.
- **Topological Phase Transitions:** Changes in the structural parameters of a photonic crystal can lead to topological phase transitions, resulting in the emergence or disappearance of topologically protected modes.
- **Robustness:** One of the characteristic features of topological photonic crystals is their robustness. Topologically protected modes are immune to local perturbations or defects, making them stable and resilient in practical applications.

I-5-5 Network parameter

It is the fundamental distance between two constituent elements. It determines the spectral region where the CP interacts with the electromagnetic wave [24].

I-5-6 The contrast of the refractive index

The refractive index (RI) of a material determines the speed of light within that material. When light travels from one material to another with a different refractive index, it changes its speed and direction [26].

I-6 Classifications of photonic crystals

I-6-1 Unidimensional photonic crystals (PhCs-1D)

The one-dimensional photonic crystal, also called "Bragg Mirrors," is represented in figure (I.8). It is a sequence of layers of different refractive indexes, periodically stacked. The behavior of the Bragg reflector is explained by the process of multiple interferences. As shown in Figure (I.9), a wave that spreads in the succession of layers undergoes reflection at each interface. This reflection is accompanied by a change of phase π if the wave moves from a medium of low index to a middle of strong index. It is carried out without phase change [21].

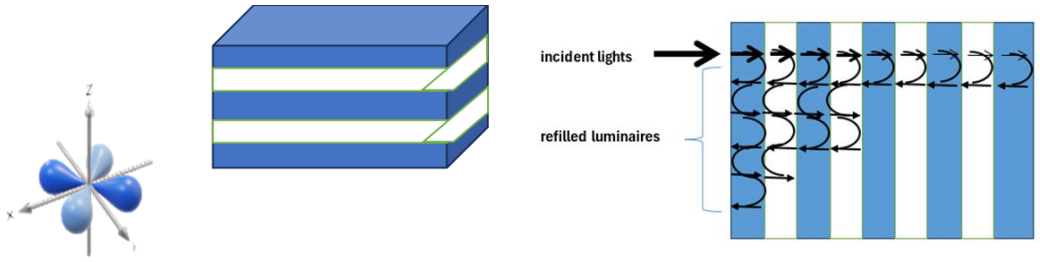

(A) (B)

Figure I.8: (A) Bragg mirror consisting of a stack of layers of thicknesses of different permittivity [21]. **(B)** Refractions of Bragg mirror [22].

This reflectivity is the manifestation of a banned photonic band. However, in 1D photonic crystals, monochromatic light is only reflected when it spreads in a direction close to the normal in the multi-layer structure.

I-6-2 Two-dimensional photonic crystals (PhCs -2D)

A two-dimensional photonic crystal is a structure that has a periodic modulation of dielectric permissiveness in two directions of space, and is homogeneous in the third. The optical properties of two-dimensional structures are heavily dependent on the polarization of [22]. electromagnetic wave. The implementation of these structures was made in several ways

(Figure I.10). For example, dielectric stems can be placed in the air (disconnected structure) or in another dialectic (connected structure) [11].

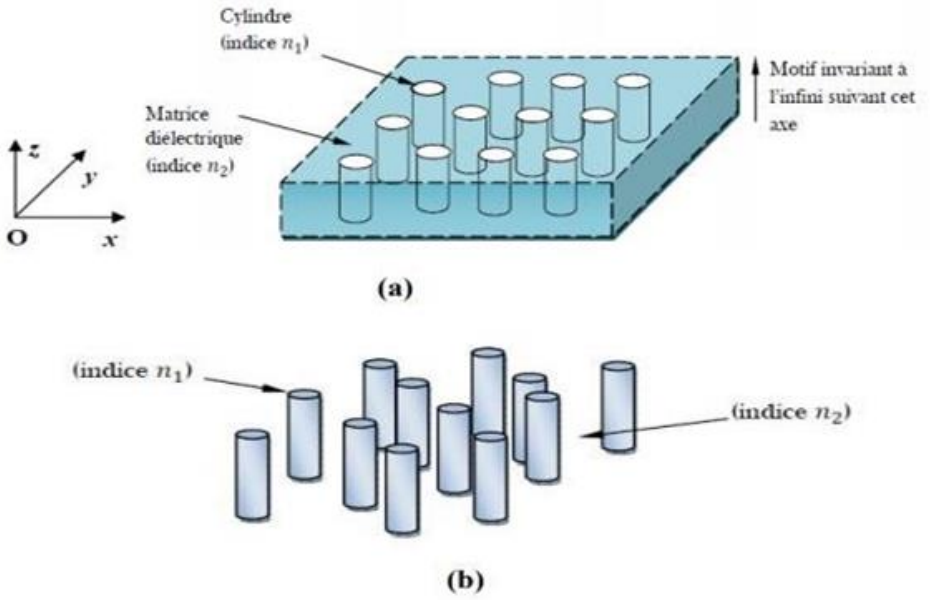

Figure I.09: Two-dimensional structures: (a) connected, (b) disconnected [20].

I-6-2-1 Physical and geometric properties of a CP-2D:

- **Index difference:** The refractive index contrast (ΔRI) is defined as the absolute difference. RI_h: High-index material refractive index of two adjacent RIs: Lo- index material Refractive Index [18]:

$$\Delta RI = RI_h - RI_l \qquad \textbf{I. 1}$$

- **Period:** In PhCs-2D, the period "a" represents the distance between the centers of two adjacent patterns. This geometric parameter, chosen according to the frequency range studied, influences the characteristics of the banned photonic band.

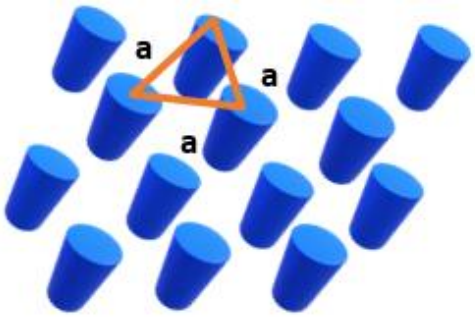

Figure I.10: The period in a disconnected 2D periodic structure [21].

I-6-2-2 Different families of two-dimensional photonic crystals

- **The square grid**: The primitive mesh is a square side "a" (Figure I.11 (a)). This type of network has been shown to be highly sensitive to the impact angle and polarization of the electromagnetic wave. It is thus difficult to obtain a total banned band, i.e., a banned tape that prevents its spread regardless of polarization. (TE, TM) [24].
- Triangular grid: The primitive mesh is an equilateral triangle on the side "a.". (Figure I.11(b)). Each node of the network is separated from its nearest neighbor by the same distance ("a"). This structure is less sensitive to the impact angle than the square grid, but the full banned band remains difficult to obtain [16].

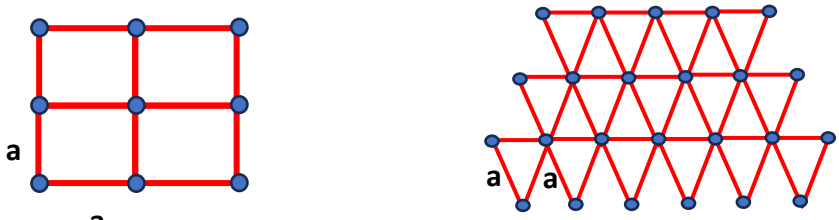

Figure I.11: (a) The square grid, **(b)** Triangular grid [16].

- **The hexagonal network:** The nitride structure of bore: If a node differs from its next node by nature or size, the crystalline structure of bore nitrite is obtained (Figure I.12(a)). The graphite structure: in this structure, all nodes are identical and spaced by a, which is similar to the crystalline structure of graphite (Figure I.12(b)) [20].

Figure I.12: (a) The graphite structure **(b)** The hexagonal network [20].

I-6-3 Three-dimensional photonic crystals

Three-dimensional photonic crystals 3D photonic crystals have attracted and still attract many research efforts. They are the only structure that produces a banned band of energy in all directions of space. The first 3D photonic crystal was manufactured by K.M. Ho *et al*. It was made of silicon spheres arranged on a diamond structure. But the story generally retains the famous Yablonovite, a 3D structure for microwaves manufactured in 1993 by E. Yablonovitch [23].

Also known as photonic crystals or photonic bandgap materials, these are periodic structures that manipulate the flow of photonics (particles of light) in a manner similar to how semiconductors control the flow of electrons. These structures are engineered to exhibit photonic bandgaps, which are ranges of frequencies or wavelengths in which the propagation of light is forbidden. This is analogous to electronic bandgaps in semiconductor materials.

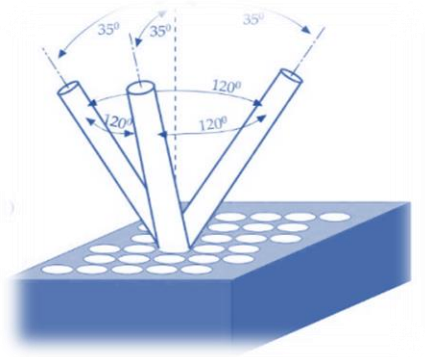

FigureI.13: The Yablonovitch [23].

I-7 Conclusion

At the end of this first chapter, we presented the basic concepts associated with photonic crystals. We needed this reminder in order to understand the behavior of PhCs-based sensors. In this context, the next chapter will be entirely devoted to PhCs-based biosensors to further improve their performance.

Chapter 11

Two-dimensional photonic crystal for optical biosensors

II-1 Introduction

Sensors that have been developed for a few decades are now adopted and widely used in all areas of everyday life (water quality and some agri-food products, biological analyses, pollution, etc.). Sensitivity, selectivity, specificity, and durability of sensors have always been key parameters in their design.

Recently, there have been several research projects using photonic crystals as a detection element due to their band structure and the confinement of light.

In this second chapter, we discuss the explanation of cavity, waveguide, and coupling in the context of photonic crystal sensors, emphasizing their crucial roles in confining light, guiding it through the sensor, and influencing resonance properties. These elements collectively contribute to the sensor's ability to detect changes in the surrounding environment, such as variations in refractive index, making it applicable for sensitive applications like biosensors.

II-2 Sensor definition

A sensor is an apparatus that converts an observed physical quantity, such as an electrical voltage, frequency, mercury height, intensity, or needle deviation, into a useful quantity [26]. A measuring device is an apparatus that produces an exploitable physical quantity under the influence of a desired physical quantity that is desired to be known and characterized. Influence quantity refers to outside dimensions that have the potential to interfere with the sensor based on their significance and kind. Temperature, pressure, humidity, and chemical concentration are the primary variables that affect these values [27].

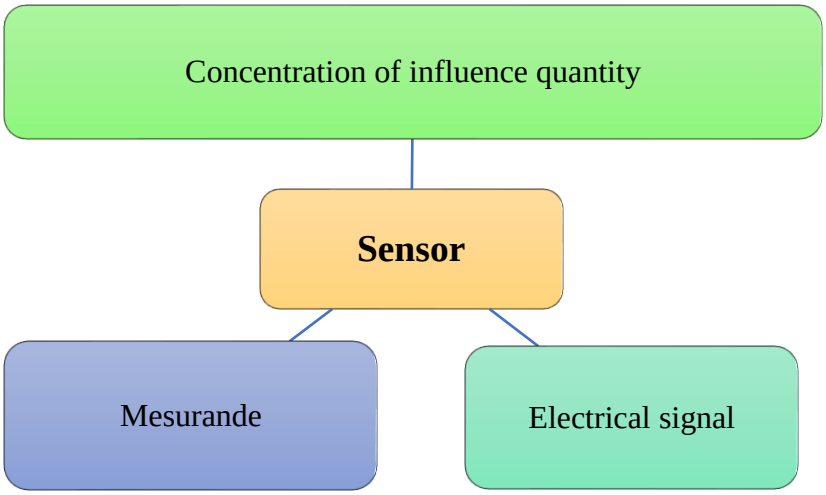

Figure II.1: Sensor proceeding work.

II-3 General parameters of sensors

Depending on the desired applications, the criteria for selecting the sensor are made taking into account the prior establishment of a load specification, which includes the type of phenomenon to be detected, the nature of the phenomenon, the quantity of the incident, etc. In order to ensure that the sensor is performing and being used in the best conditions, its metrological characteristics must be taken into account [28]. In this part, we will present a reminder of the definition of the most important metrological characteristics of a sensor:

II-3-1 Calibration of sensor

Calibration of sensors allows the adjustment and presentation of the relations between the measurement quantity (measurement) and the electrical output quantity in graphical or algebraic form [29, 30].

$$s = F(m). \qquad \textbf{II.1}$$

- F(m) The function of sensor input quantity
- (s) Output quantity

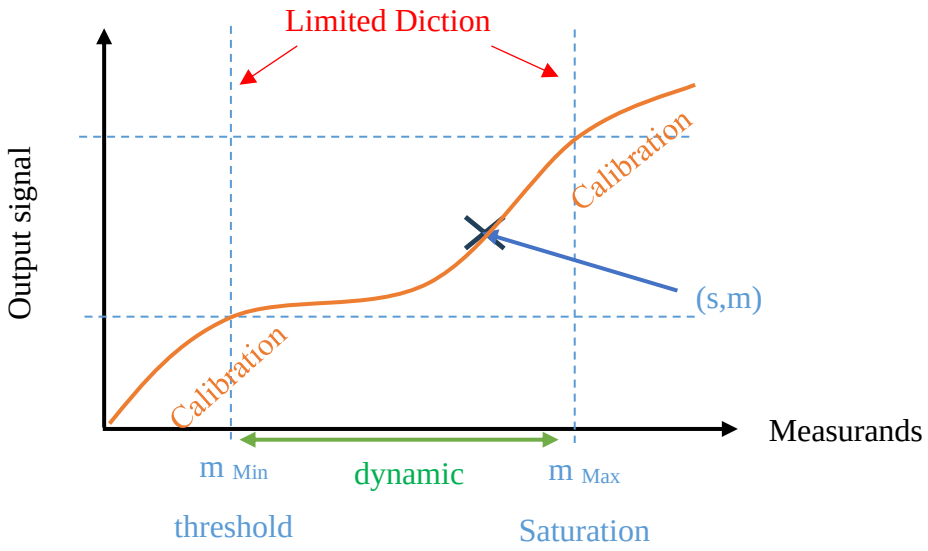

Figure II.2: Calibration of sensor [30].

→ **Detection Limit (LD)**: The detection limit represents the minimum value of the quantity being measured that the sensor can reliably detect. It's the point at which the sensor's response becomes distinguishable from background noise. Going below this limit results in unreliable measurements [31].

→ **Saturation:** On the other end of the spectrum, saturation occurs when the sensor reaches its maximum value [32].

→ **Calibration:** The sensor's calibration curve (as shown in Figure II.2) helps define this working range. Calibration ensures that the sensor responds correctly to different quantities under specific conditions.

II-3-2 Sensor sensitivity

Sensor sensitivity is a parameter that represents the change in the output signal depending on the variation of the meter [33]. It is defined as the ratio between the variation of the output signal and the variance of the measuring (m) (inclination of the linear portion of the calibration curve). It is expressed by the relation:

$$S = \frac{\Delta S_{out}}{\Delta m} \qquad \textbf{II.2}$$

II-3-3 Response time or speed

Rapidity is the ability of a sensor to track time variations in the measuring range. It corresponds to the time required for the sensor to deliver a certain portion of the signal's full amplitude [34].

In recent years, the development of electrical sensors has given rise to high-performance devices that can be used in various fields as a result of increased requirements for miniaturization, information processing time, reduced losses, and reduced pollution. Currently, we can distinguish several optical sensors. Photonic crystals Their detection techniques are based on the variation of information characterizing the light wave, such as the change in light intensity, the variation in time coherence, and phase variation [35].

II-4 Biosensor definition

A biosensor is an analytical system that exploits the biological detection capacity of a target molecule in conjunction with a physicochemical transducer that transforms biological recognition into a physically measurable signal. It is composed of three main elements: a sensitive biological layer, a transducer, and an output. signal. The biological layer contains a bio-receptor, which recognizes the desired biological species and is immobilized on the transducer. This last step ensures the conversion of the biological response into a physical phenomenon. At the highest cloud, the output signal allows the measurement of the physical phenomenon developed by the transducer. This cloud often contains steps for amplification and display that are appropriate and user-interpretable [35].

II-5 Principle of biosensor

A biosensor is a specialized analytical device that combines a biological component (a bioreceptor) with a physicochemical transducer to detect the presence or concentration of a specific biological analyte. The design and principles of biosensors involve several key components [30].

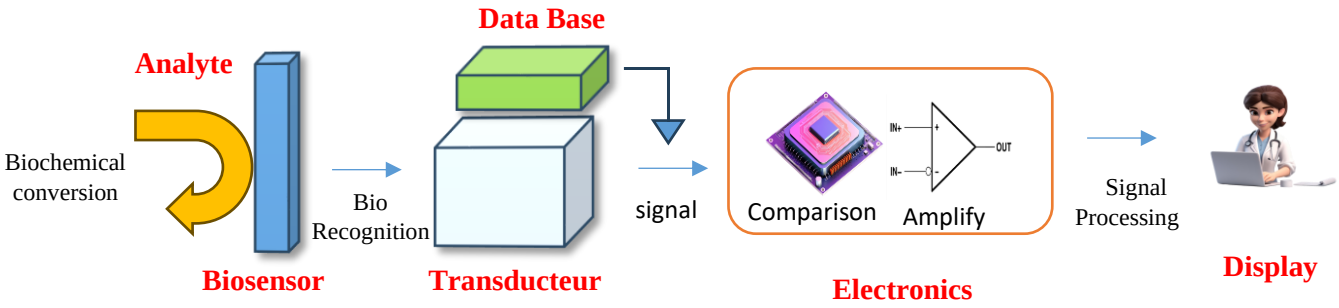

Figure II.3: Schematic diagram of typical biosensor consisting of bioreceptor.

The bioreceptor is a crucial element in biosensor design. It is a biomolecule or biological entity that interacts selectively with the target analyte. Common bioreceptors include [26]:

- Enzymes: Catalyze reactions with the analyte.
- Antibodies: Bind specifically to antigens.
- DNA/RNA: hybridize with complementary sequences.
- Cells react to specific substances or toxins.

The transducer is responsible for converting the biochemical signal generated by the bioreceptor into a measurable and often electrical signal. Key types of transducers include [28]:

- Electrochemical Transducers: Measure changes in electrical properties (e.g., potentiometric, amperometric, conductometric).
- Optical Transducers: Detect changes in light properties (e.g., fluorescence, absorbance, surface plasmon resonance).
- Piezoelectric Transducers: Measure changes in mass affecting acoustic waves.
- Thermal Transducers: Monitor changes in temperature resulting from biochemical reactions.

The specificity of the biosensor relies on the interaction between the bioreceptor and the analyte. This interaction generates a signal proportional to the concentration of the analyte. For example [27]:

- Enzymes catalyze reactions, producing measurable products.
- Antibodies bind specifically to antigens, creating a detectable complex.
- DNA-RNA hybridization results in a change in electrical properties.

The biosensor's output signal is processed and often amplified for accurate measurement. Signal processing may involve [29]:

- Amplification: Enhancing weak signals for better detection.
- Filtering: removing unwanted noise from the signal.
- Conversion: Transforming the signal into a format suitable for display or further analysis.

The display unit is composed of a user interpretation system, such as a computer or a printer, that generates the output so that the corresponding response can be readable and understandable by the user.

II-6 Classification of biosensors

Biosensors can be classified based on several criteria, including the type of biological recognition element, the transduction mechanism, and the application. Here is a classification of biosensors [36]:

Table II-1 : Classification of biosensors [19]

Based on Biological Recognition Element	Enzymatic biosensors	• Use enzymes as the biological recognition element. • Enzyme-substrate reactions produce a measurable signal. • Common for glucose, cholesterol, and ethanol detection.
	Immunosensors	• Employ antibodies or antigens as recognition elements. • Used for the detection of proteins, pathogens, and antibodies. • Common in clinical diagnostics and environmental monitoring.
	DNA Biosensors	• Utilize DNA or RNA strands as recognition elements. • Detect nucleic acids or specific sequences. • Widely used in genetic testing and pathogen identification.
	Cell-Based Biosensors	• Use living cells as the recognition element. • Monitor cellular responses to environmental changes. • Applied in toxicity testing and environmental monitoring
Based on Transduction Mechanism	Electrochemical Biosensors	• Measure electrical changes (current, voltage, impedance). • Include amperometric, potentiometric, and conductometric biosensors. • Common in glucose monitoring and DNA detection.
	Optical Biosensors	• Rely on changes in light properties (absorbance, fluorescence, surface plasmon resonance). • Used in label-free detection and imaging. • Applications in environmental monitoring and medical diagnostics
	Piezoelectric Biosensors	• Measure changes in mass affecting acoustic waves. • Common in mass-sensitive applications. • Applied in monitoring molecular interactions.

	Thermal Biosensors	• environmental monitoring. • Monitor changes in temperature resulting from biochemical reactions. • Include calorimetric biosensors. • Used in medical diagnostics and
Based on Signal Output	Continuous Monitoring Biosensors	• Provide real-time and continuous data. • Used in applications where dynamic monitoring is essential.
	Discrete Monitoring Biosensors	• Provide specific, discrete measurements. • Common in point-of-care testing and rapid diagnostics.

II-7 Pathogen detection

Photonic crystal sensors have been applied in various fields, including medical diagnostics, environmental monitoring, and food safety.

Keep in mind that the field of photonic crystals and their applications in sensing is dynamic, and there may be ongoing developments and improvements in technology. If you have specific details or a particular aspect of photonic crystal-based pathogen detection you'd like more information on, feel free to provide additional context [37].

Pathogens and its types Pathogens are infectious agents that causes diseases, our body has immune systems that fights against pathogens but some pathogens are strong enough to defeat human immune system. There are many kinds of pathogens, severity of disease depends on the type of pathogens [37]. Main types of pathogens are as follows [38]:

- Bacteria- it is microscopic and reproduces rapidly when it enters the body, it releases toxic substances damages tissues and causes illness.
- Virus- size of virus is smaller than bacteria; conquers host cell replicates producing hundreds and thousands of new born viruses infecting a greater number of host cells. Virus spreads very fast from person to person through air, blood and body fluids.
- Fungi- it has evolving capacity; fungus has lot of species causes diseases in human beings. Common fungal disease is ringworm in skin.
- Protists are single-cell organisms; they infect another organism and make it difficult to survive. These pathogens mainly affect the food chain, and they also cause infections in the intestine, resulting in diarrhea.
- Parasitic worms: these types of pathogens are a little large in size and are visible with the naked eye. It lives in different parts of our body; for example, tapeworm lives in the intestine.

II-8 Two-dimensional photonic crystal for optical biosensors

In this part, we are talking about the history's application. Two-dimensional photonic crystal for optical biosensors Plasmonic biosensors:

II-8-1 Plasmonic biosensors

Two-dimensional photonic crystal biosensors have been extensively studied and developed for plasmonic sensing.

- In 2022, a paper discussed optical biosensors using plasmonic and photonic crystal band-gap structures for the detection of basal cell cancer. These structures are composed of one-dimensional photonic crystal (PC) lattices coupled to two metal-insulator-metal (MIM) plasmonic waveguides [38]. The maximum obtained sensitivities and FOM values of the designed biosensors are equal to 718.6, 714.3 nm/RIU, and 156.217, 60.1 RIU^{-1}, respectively [39].

- In 2023, an innovative biosensor harnessing the potential of photonic crystal technology to identify a multitude of cancer cells was reported. The design showed improvement in the three judgment factors (i.e., compactness, quality factor level, and sensitivity) by approximately 440%, 170%, and 110%, respectively, compared to the highest levels extracted from relative literature [40].

II-8-2 Biosensors in cancer detection

Two-dimensional photonic crystal biosensors have been extensively studied and developed for cancer detection.

- In 2024, a two-dimensional microcavity ring with a waveguide structure was designed and simulated to sense the existence of malignant cells in the bioanalyte. The highest sensitivity of 995 nm/RIU with a Q-factor of 70 was achieved [41].

- In 2023, a novel design of a biosensor based on silicon photonic crystal double-elliptical ring resonators with improved sensitivity for cancer detection was proposed. The design obtained simultaneous high sensitivity of 1170 nm/RIU and 1116.66 nm/RIU and improved quality factor (Q) of 422.36 and 449.16 for skin (Basal) and cervical (HeLa) cancer cells, respectively [42].

- In 2023, an innovative biosensor harnessing the potential of photonic crystal technology to identify a multitude of cancer cells was reported. The design showed improvement in the three judgment factors, quality factor, and compactness for healthy cells: 455.33 nm/RIU, 7199.86, and $9.4 \times 5.5\ \mu m^2$, respectively [43].
- In 2022, a highly sensitive plasmonic photonic crystal fiber (PCF) biosensor was reported for cancer cell detection. The highest sensitivity of 410 nm/RIU, with a Q-factor of 30 [44].

II-8-3 Glucose Sensors

Two-dimensional photonic crystal biosensors have been extensively studied and developed for glucose sensing.

A review paper discussed optical methods for continuous glucose monitoring, including near-infrared (NIR) spectroscopy, mid-infrared (MIR) spectroscopy, Raman spectroscopy, photoacoustic (PA) spectroscopy, fluorescence technology, optical coherence tomography (OCT), holographic technology, and hydrogel sensing technology [46].

II-9 Refractive index sensor based on photonic crystals

The general concept of label-free optical detection relies on the alteration of one of light's characteristics when it comes into contact with the object of interest. Several detection techniques are available for this, such as those that take advantage of changes in the index of refraction, absorbance properties, or non-linearity. In the following, we will only be interested in detection based on index change [47]. Measuring the variation in the analytical environment's refractive index around the interface with the evanescent electromagnetic field is the basis of this type of detection. Generally speaking, the electromagnetic field is concentrated in the highest index region and decreases exponentially beyond the sensor-environment interface, extending several hundred nanometers toward that point [48].

In previous years, refractive index sensors have been thoroughly researched and increasingly popular. The detection functions applied to photonic crystal structures produce a large confinement of light in the analytic substance to be detected). The principle of such detection is to measure the variation in the refraction index of a sensitive element depending on the presence of an analytic. So, to make the sensor very sensitive to a small variation in the refraction index, it is necessary to produce a large interaction between light and matter by concentrating light in a very small volume [49].

Several devices have been proposed as refractive index sensors using different types of photonic crystal structures, such as CPh cavities, waveguides, and the and the coupling of a waveguide with a cavity.

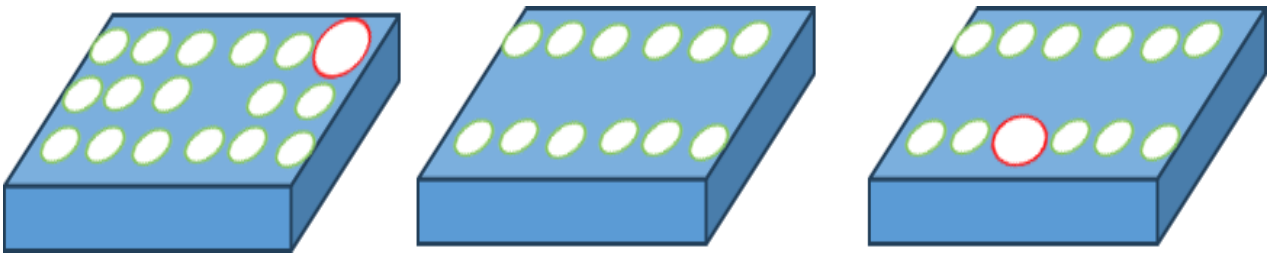

Figure II.4: PhC cavities, waveguides, coupling [17].

The refraction index n of a transparent and homogeneous medium is the ratio of the velocity of light from the vacuum c to the speed of light in the studied medium λ.

$$n = \frac{c}{\lambda} \qquad \text{II.3}$$

The refraction index is a unified measure. For a liquid: 1.3 < RI < 1.7

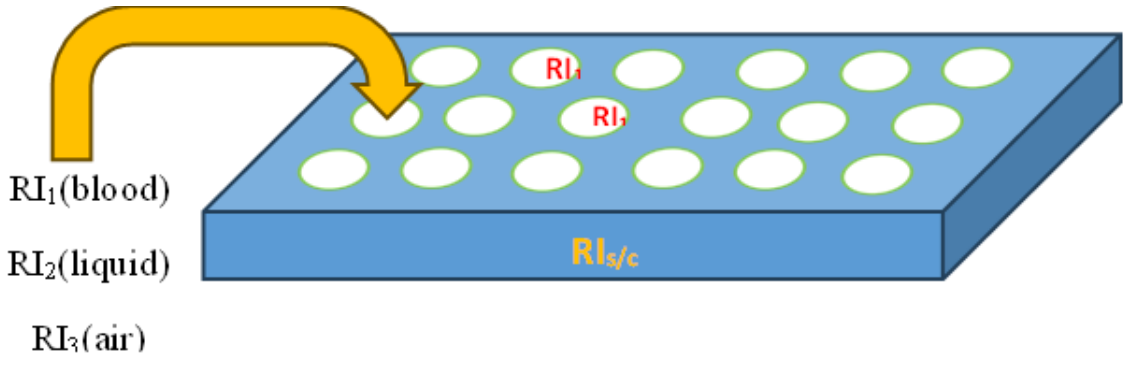

Figure II.5: Photonic crystals sensor Base Refractive index

II-9-1 Cavity-based refractive index sensor

Due to the different types of structures, cavity architecture presents a very interesting area of current research due to the compact quantity of these components, their high-quality factor, and their sensitivity. The quality factor (Q) and sensitivity (S) illustrate the performance of a cavity at CPhs for detection applications.

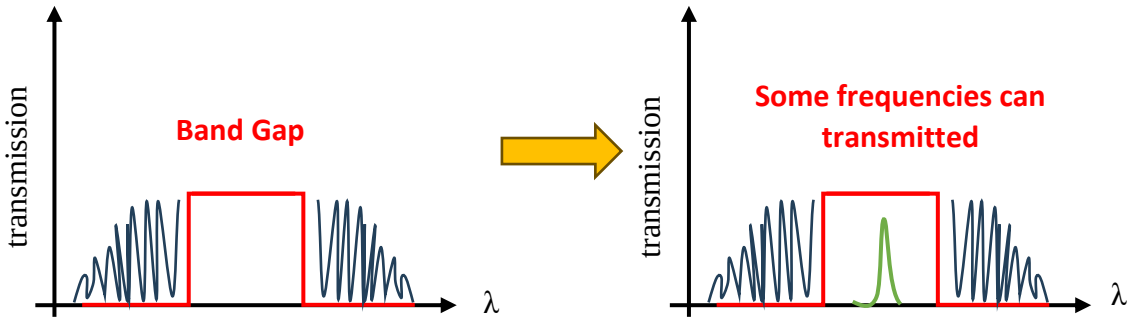

Figure II.6: Band gap before and after cavity insertion

- **The quality factor** describes the sharpness of the resonance; it represents the strong confinement of light in the cavity, and it is defined by the resonant wavelength and δλ the width at the middle height of the peak.

$$Q = \frac{\lambda 0}{\delta\lambda} \qquad \text{II.4}$$

- **The sensitivity** is expressed by Δλ is the variation of the wavelength and Δn the change of the refraction index.

$$s = \frac{\Delta\lambda}{\Delta n} \qquad \text{II.5}$$

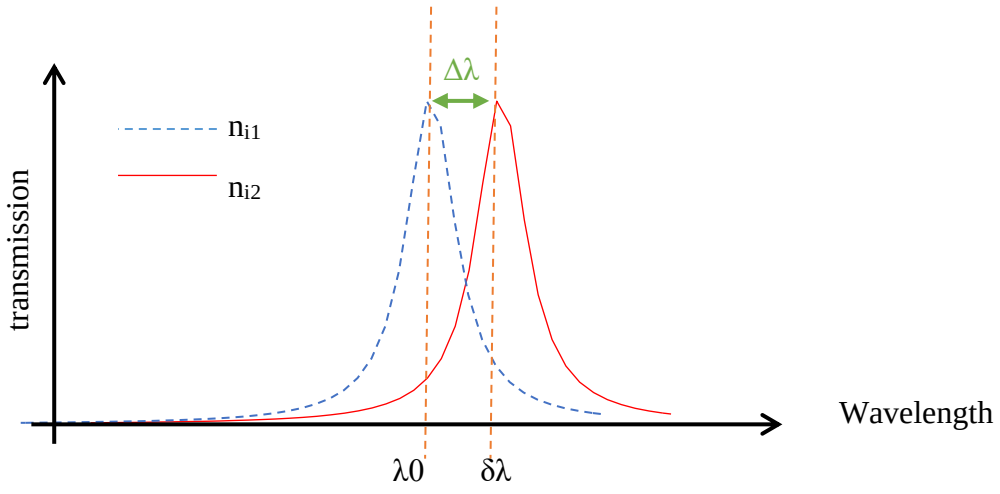

Figure II.7: Refraction index sensor based waveguide structure.

II-9-2 Waveguide-based refraction index sensor

The application of photonic crystal waveguides as a refraction index sensor is of great interest, as they are able to act directly as a detection element without the design of an integrated cavity. The realization of the waveguide at CPh is usually achieved by introducing a linear defect in the periodic structure.

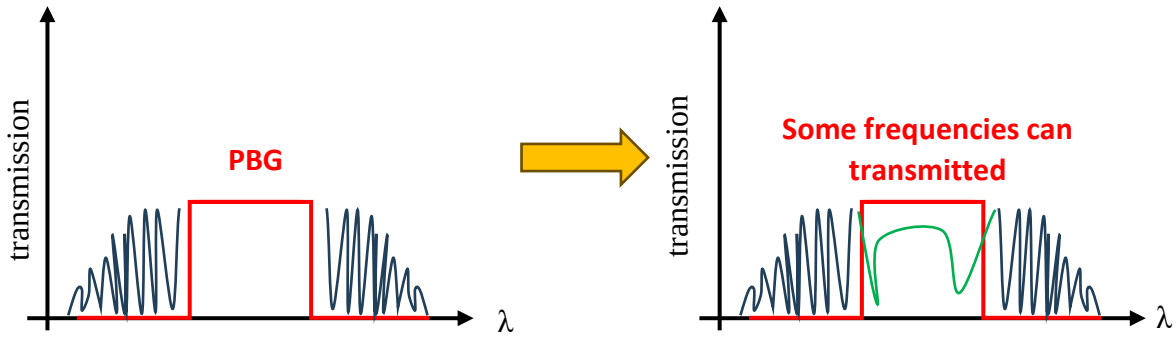

Figure II.8: Band gap before and after waveguide insertion

The most common spectral characteristic used in a CPh waveguide is the cutting wavelength (λ_{cutoff}). The latter describes the maximum wavelength at which the optical mode can propagate in the CPh waveguide. So, the detection principle is based on λ a cutoff variation depending on the variation of the refraction index.

$$s = \frac{\Delta\lambda cutoff}{\Delta n} \qquad \text{II.6}$$

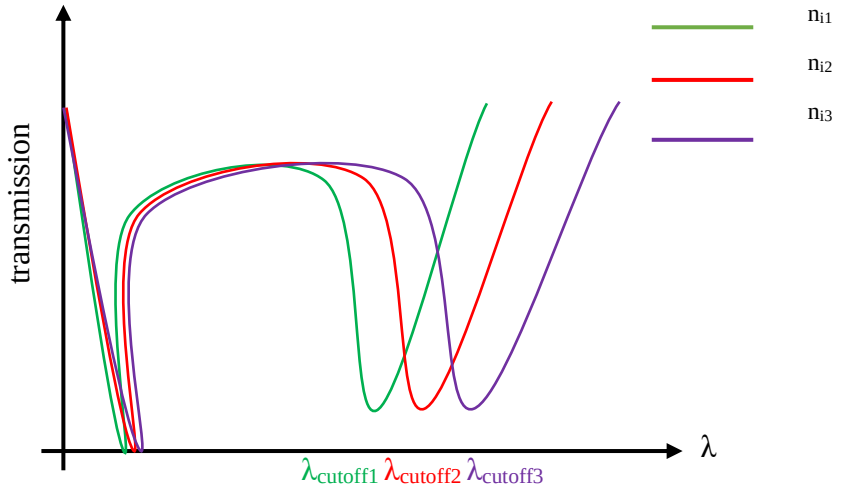

Figure II.9 Transmission spectrum of refractive index sensor (Waveguide) .

II-9-3 Refractive index sensor based on side coupling

In this part, we will study a coupling path that consists of juxtaposing the cavity parallel to the guide to obtain a side interaction of cavity modes with the guide modes.

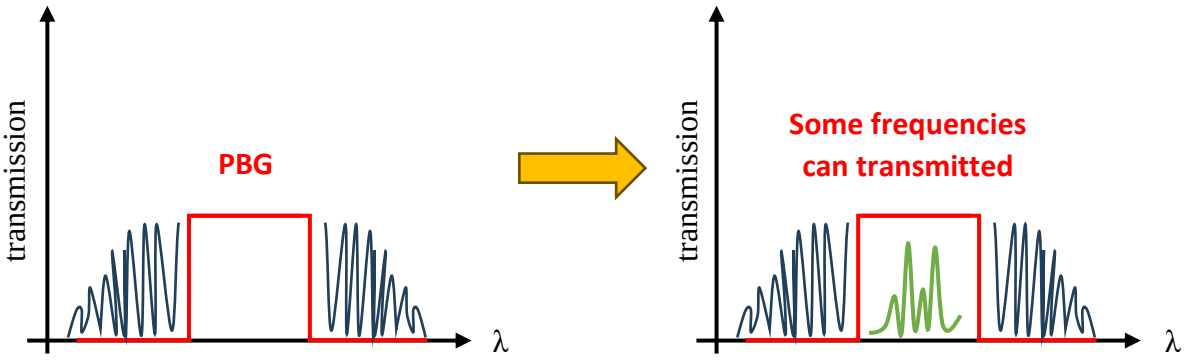

Figure II.10: the 'PBG' before and after the coupling

II-10 Conclusion

In this chapter, we have presented, refractive index biosensor based on photonic crystal, where the refractive index set as a parameter to design optical biosensor devices using photonic crystals. Such optical biosensor devices have high sensitivity and quick response time for small variations in samples. Special emphasis is placed on the integration of photonic crystals with biological elements to enhance sensing capabilities and responsiveness. The chapter highlights the results arising from the use of this technology in various fields, such as biomedicine.

CHAPTER III

Design and simulation of 2D photonic crystals sensors for bio-detections

III-1 Introduction

Over the past few decades, Photonic crystals (PhCs) have attracted the interest of several researchers, leading them to design and create a variety of optical sensors, because of their simple periodic dielectric structure with periodic spatial distribution of refractive index. Due to their unique properties, PhCs have been crucial in the design of all-optical circuits. One of these features is the appearance of a photonic bandgap (PBG), which blocks specific wavelengths from passing through the lattice in one, two, or any number of polarization directions inside the PhC structure. By introducing defects to the periodic PhC structure (either a point or a line defect), the PBG property may be changed. Additionally, by controlling the light flow inside the structure, a specific prohibited wavelength can be propagated across the periodic structure.

In this context, a novel highly sensitive 2D refractive index biosensor based on PhCs for detecting brain cancer is developed and introduced. In general, our results revealed that the proposed device has appreciable potential to be used as a powerful tool to distinguish accurately between normal and abnormal brain tissues.

III-2 Presentation of RSoft photonic design software

RSoft is a fundamental program in photonic software, enabling researchers to design various optical devices such as waveguides, resonance cavities, and optical circuits. The software calculates diffraction without providing reflection or transmission, and its key advantages include an easy-to-use Computer-Aided Design (CAD) interface, allowing precise definition of arbitrary profiles with a rough approximation for quickly obtaining improved results.

The RSoft CAD software serves as a foundational tool for managing passive modules like Beam Rob, Diffract Mod, FullWAVE, Band Solve, and Grating Mod. Specifically, the BandSolve and FullWAVE modules are dedicated to simulating photonic crystals. Figure III-1 illustrates the graphical interface window for RSoft photonic design software.

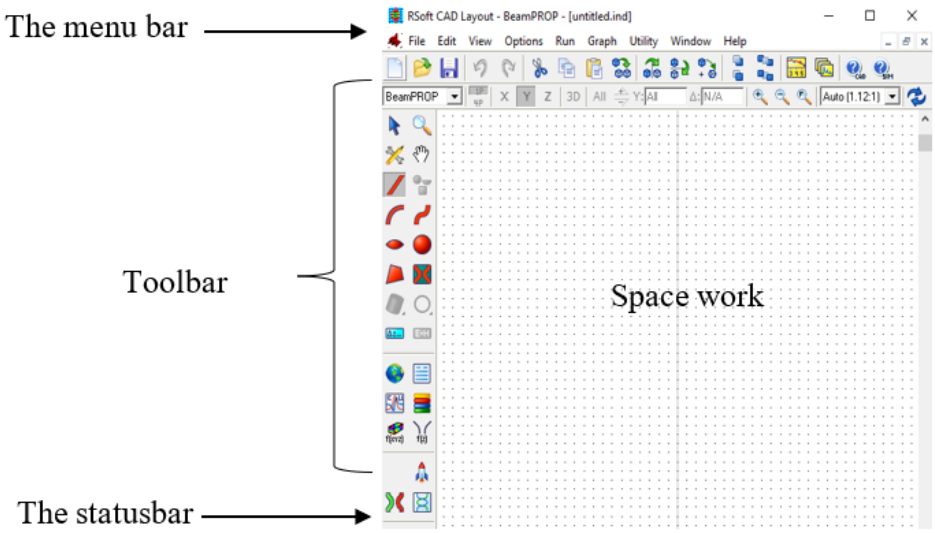

Figure III-1: Graphical interface window for RSoft photonic design software.

III-2-1 Modeling methods of PhCs

When it comes to complex structures consisting of several types of materials with different refraction indices (RIs), the numerical modeling of the electromagnetic properties of the material is delicate. In fact, solving Maxwell's equations in these systems is very difficult. In these cases, the use of numerical calculation methods is essential. The FDTD method is one of the existing methods proposed by Yee in 1966 [50].

The interest of the FDTD method lies in the simplicity of its principle of operation and in the large amount of electromagnetic information that can be derived from the modeling system. The core of this method is first to discretize the structure in regular and fine mesh, and then to approximate the equations to the partial derivatives of the fields by finite differences. Field components can be calculated at any point in the structure and at any time.

III-2-1-1 The BandSOLVE Simulator

The BandSOLVE simulator is a software for calculating photonic energy bands using the PWE method. All band diagrams in our study were calculated using RSoft-CAD's "BandSOLVE" module. It is a simulation software capable of generating and analyzing photon energy band diagrams. The calculation of diagrams is based on the method of decomposition of electromagnetic fields in plane waves for periodic structures [51].

In 2D, two different propagation directions are to be considered: the TE and TM polarizations, these polarisations are disconnected and two independent band diagrams are made. In either case, there is no photonic band gap (PBG). BandSOLVE is generally needed to improve the properties of PhCs structures, these properties are simulated by the FDTD method

implemented in the FullWAVE module, to verify time-related properties, such as losses, and to calculate the distribution of the field in a finite-dimensional structure. In addition, it can be applied to structures such as photonic crystal fibers, which are complex for other simulation techniques [38].

III-2-1-2 The FullWAVE Simulator

The FullWAVE simulator is a software suite developed by RSoft. It is based on the FDTD method. The goal of using FullWAVE is to obtain a set of simulations to calculate the spread of light in waveguides with arbitrary geometries. This software is well suited to our simulations as it allows the design of complex photonic structures. FullWAVE is ideal for studying the propagation of light for a wide variety of photonic structures.

III-3 Presentation of The Host Structure

We are interested in transmission through a periodic crystal formed by cylindrical air holes in a silicon substrate. These inclusions are arranged according to a triangular grid. The central row can be filled with a liquid for which we want to probe the acoustic and optical speeds of sound and light. The radius of the central line may also be different from the others. The objective is to define a structure that should be highly sensitive to both the change in the refraction index and the speed of the sound of liquids in order to be applied to the detection of a large number of biological elements.

It is not simple to create a biosensor based on PhCs. It stands to reason that you should search for a configuration that maximizes interaction. This indicates that in order to get the desired result, a number of parameters need to be chosen. Therefore, in order to get such dimensions, computer simulations must be run (Figure III-2).

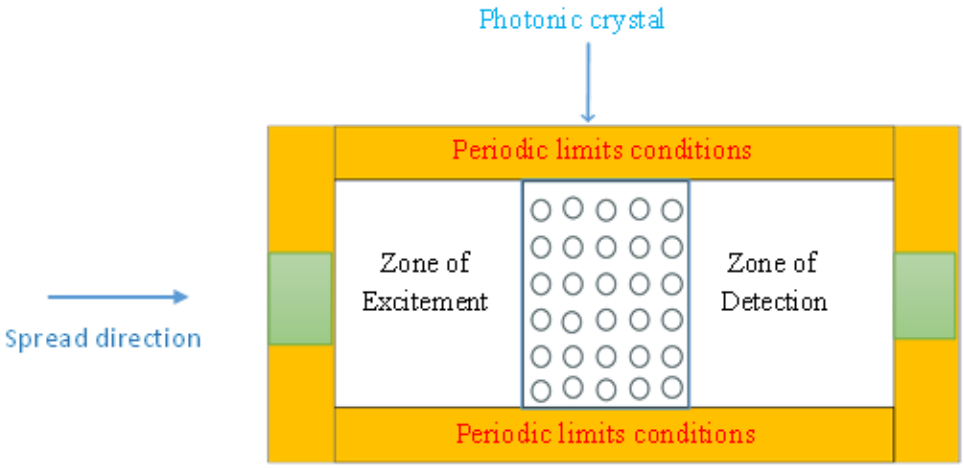

Figure III-2: Periodic boundary conditions around all structure.

Before designing our biosensor, we start by studying the proposed 2D-PhC structure, in order to determine the band diagram of the proposed 2D-PhC structure. the proposed structure is constructed in a silicon-on-insulator (SOI) substrate because of the strong light-matter interaction. The size of the used photonic crystal structure is (21×19), the structure design is presented as shown in Figure III.3. It consists of a 2D hexagonal lattice of air where the radius of the air holes r=0.19 µm. The lattice constant (a) is considered as 0.47 µm, and the index profile of Si slab n_{si}=3.42.

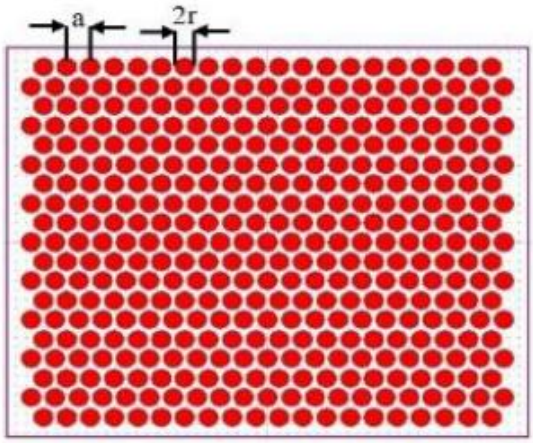

Figure III-3: Schematic of the proposed 2D-PhC structure.

III-3-1 Steps of working using RSoft software

- Simulation of a triangular structure with air hole grid (21×19);

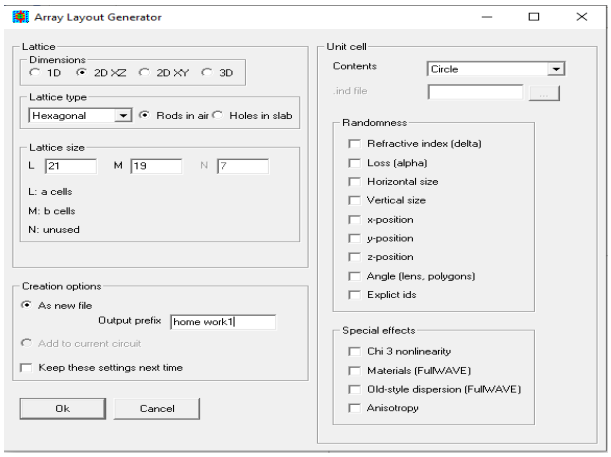

Figure III-4: Array layout generator.

- The network settings are given as follows: the period a=0.47 µm, the radius of the air holes r=0.19 µm:

- Select the value of the period (a=0.47 µm):

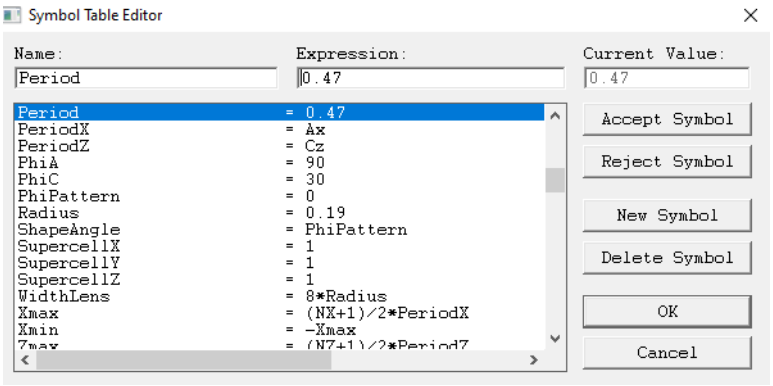

Figure III-5: Symbol table editor (Select the period value).

- Select the value of the air hole radius (r=0.19 µm):

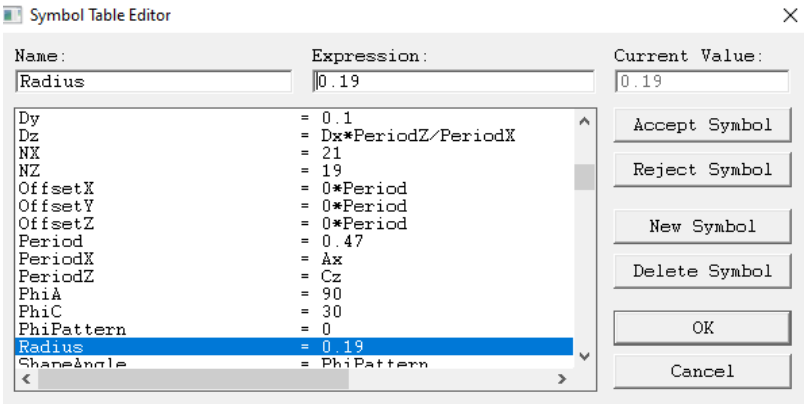

Figure III-6: Symbol table editor (Select the radius value).

- Choose the value of the high index dielectric (n_{si}=3.42) and the central wavelength of the open space used is 1550nm as this wavelength is suitable and well-known for biosensing purposes.

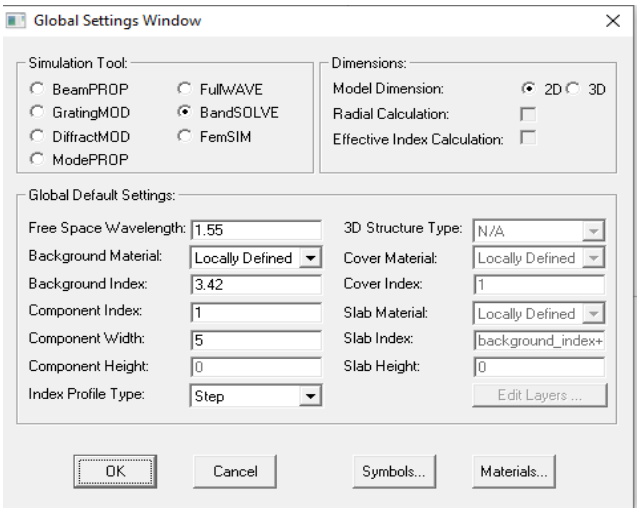

Figure III-7: Global settings windows.

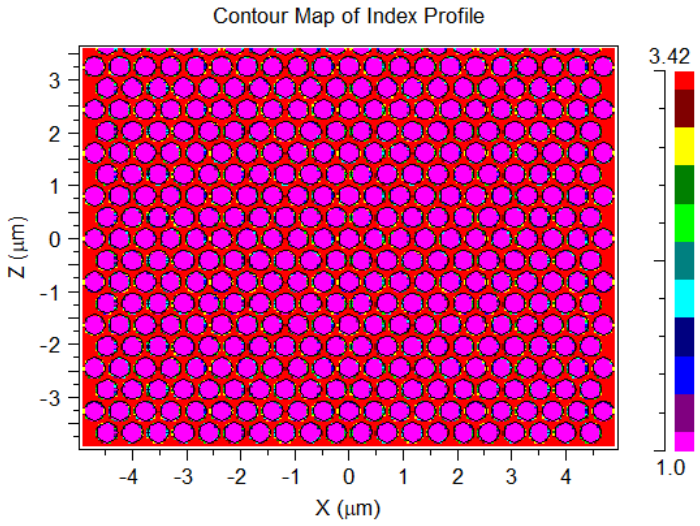

Figure III-8: Distribution of the refractive index of a hexagonal photonic crystal.

III- 4 TE and TM polarizations in a photonic crystal

The 2D photonic crystal contains two polarizations TE (electric transverse) and TM (magnetic transverse). The TE polarization (or transverse magnetic TM) is defined when the magnetic field vector H (or electrical E) is parallel to the air cylinders of the network in question. Thus, a banned band completed simultaneously for both polarizations is only possible for a very high air filling factor.

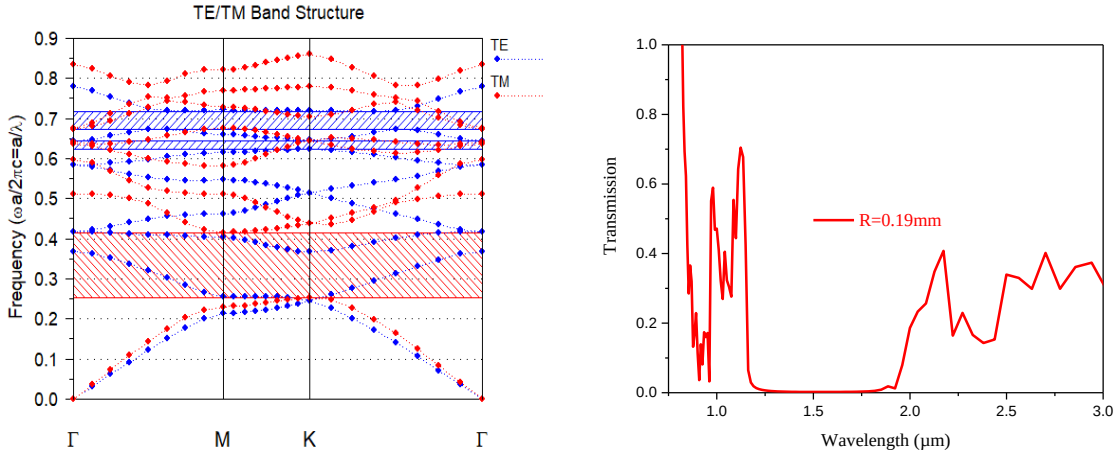

Figure III-9: (a) Band diagram of the proposed 2D-PhC structure; (b) The transmission spectrum of the structure calculated by 2D-FDTD.

The parameters of the hexagonal air hole structure are chosen to open a forbidden band across the range of the desired wavelength. Typically, we want to open a forbidden band for TM mode around interest frequencies. The proposed structure has a large bandgap (PBG) in the

wavelength range of 1330-2189 nm for a TM-polarized wave, which is calculated by the 2D-PWE method of BandSolve software (Figure III-9).

Table III-1: The presentation of PBG (TE_1, TE_2, TM).

PBG_1=0.2365µm	**PBG_2=0.1132µm**	**PBG_3=0.85µm**
TE_1	**TE_2**	**TM**
f_1=0.71784	f_1=0.64437	f_1=0.416
f_2=0.67292	f_2=0.62287	f_2=0.25272
λ=f/a	λ=f/a	λ=f/a
λ_1=3.7781	λ_1=3.3914	λ_1=2.1894
λ_2=3.5416	λ_2=3.2782	λ_2=1.33

III-4-1 Effect of hole radius on the performance of the PhC structure

In order to investigate the performance of the proposed PhC structure, we fixed the value of the refractive index (n=1) and change the hole radius from 0.17µm to 2µm with a step of 0.01µm. It is well noted that decreasing the radius of air holes lead to a redshift of the wavelength, and vice versa (Figure III-10).

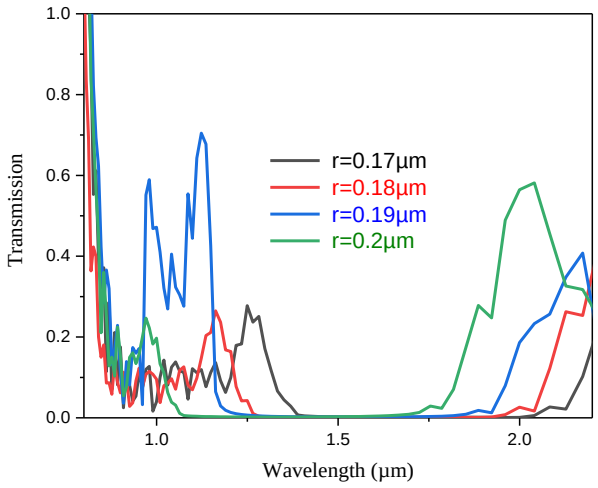

Figure III-10: Normalized transmission spectrum of the proposed design as a function of wavelength for different hole radius (r=1.7,1.8,1.9 and 0.2µm) for n=1.

Now, we investigate the performance of the proposed PhC structure but by changing the hole radius from 0.17µm to 2µm with a step of 0.01µm for n=1.33 (refractive index of water). It is well noted also that decreasing the radius of air holes lead to a redshift of the wavelength,

and vice versa (Figure III-10), besides the PBG is tighter for n=1.33 compared to n=1. Thus, we choose the value of hole radius equal to 0.19µm due to its high BPG (Figure III-11).

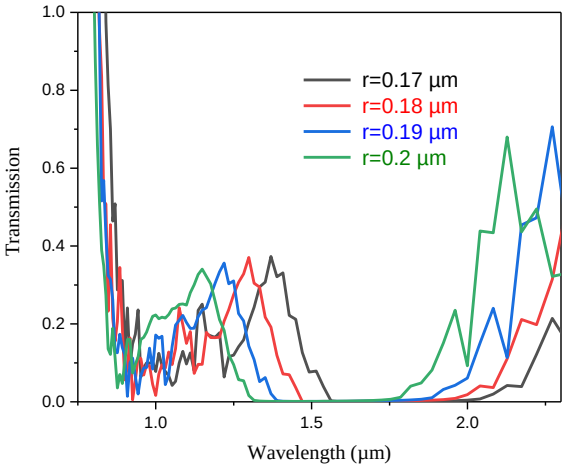

Figure III-11: Normalized transmission spectrum of the proposed design as a function of wavelength for different hole radius (r=1.7,1.8,1.9 and 0.2µm) for n=1.33.

III-5 The Waveguide Characteristics

Introducing certain defects such as point defects as cavities or line defects as waveguides, and their coupled elements in the structure can adjust the dispersion diagram hence permit to particular modes to propagate in the bandgap [52]. To break the periodicity of our proposed structure and localize the light, a photonic crystal waveguide W1 is created by removing one row of air holes in the ΓK direction as depicted in Figure III-12.

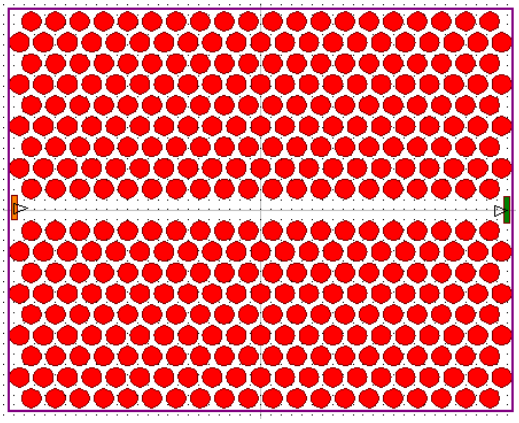

Figure III-12: Design of the waveguide formed by the omission of a row of air holes.

The corresponding wavelength of the resonance peak in extinction spectrum is called resonance wavelength λ_{res}. The refractive index sensitivity S is defined by the ratio of the resonance wavelength sift $\Delta\lambda_{res}$ to the change of refractive index of surrounding medium Δn [53].

$$S = \frac{\Delta\lambda_{res}}{\Delta n}$$

Figure III.13 shows the normalized transmission spectrum of the W1 waveguide for different refraction indices (RIs), calculated using the 2D-FDTD method. The TM mode transmission spectrum shifted to larger wavelengths with the increase in refraction index (RI) from 1 to 1.4 with an increment of 0.1. We can clearly note that the shift of the cutting wavelength (λcutoff) obtained is almost linear, and when the refraction index (RI) increases from n=1 to 1.4, which corresponds to a sensitivity (S) of 127.5nm/RIU (Table III-2).

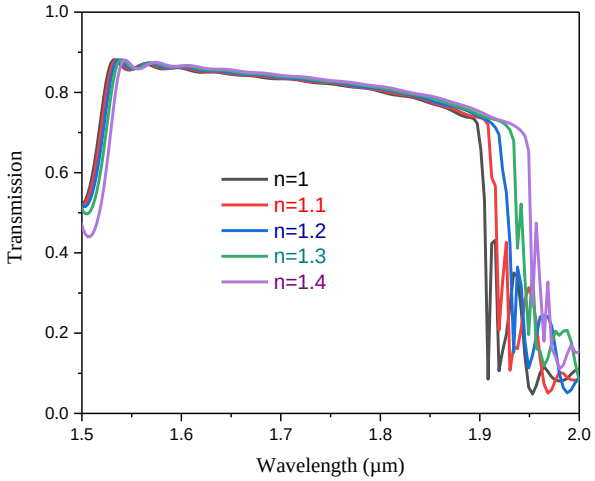

Figure III-13: Normalized transmission spectrum for different refraction indices (RIs) ranging from n=1 to n=1.4 with an increment of Δn=0.1.

The comportment of the designed sensor is analyzed using the finite-difference time-domain (FDTD) method from the RSoft software package.

Table III-2 : The sensitivity of the proposed design for different RI.

RI	λ_{cutoff} (µm)	Sensitivity (nm/RIU)
1	1.9083	X
1.1	1.9195	112
1.2	1.9338	127.5
1.3	1.9382	99.66
1.4	1.953	111.75

III-6 Design of the proposed capsule-shaped biosensor

It is well known that the periodicity of the dielectric function of a PhC is broken if defects are introduced into its periodic lattice structure. Consequently, to break the periodicity of the structure and localize the light, two photonic crystal waveguides W1 are created by removing one row of air holes in the ΓK direction, and a capsule-shaped defect was symmetrically positioned into the center of the structure by removing eleven lattice holes, to form one capsule-shaped cavity, while decreasing the radius of four specific holes near the microcavity, and by separating the capsule-shaped cavity and the two waveguides by three holes to generate localized optical modes that resonate in this microcavity (Figure III-14).

It is important to note that the infiltration is total, where all holes are totally injected with the analyte.

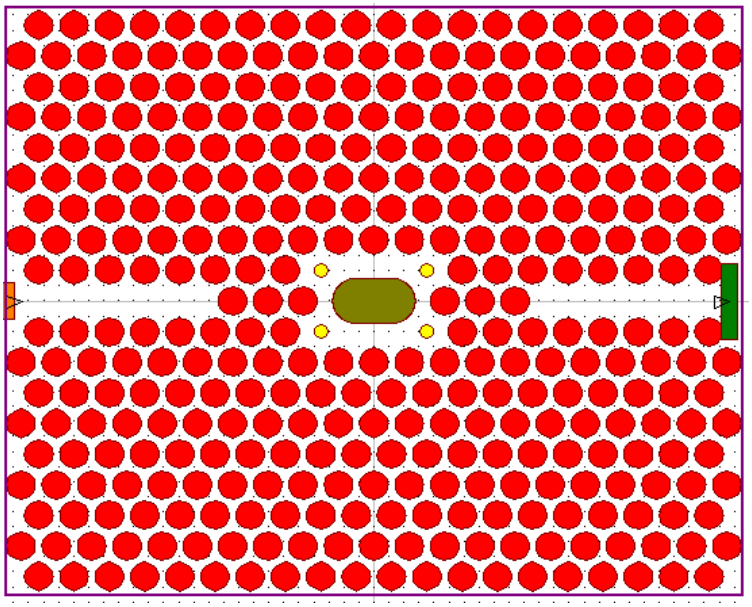

Figure III-14: Schematic of the capsule-shaped 2D-PhC sensor.

III-6-1 Performance of the proposed capsule-shaped biosensor

Figure III.15 represents the normalized transmission spectrum of cavity coupled waveguide (Air is selected as an analyte (n=1)) obtained using the FDTD method. As can be seen, when the microcavity is in resonance state, four transmission peaks are observed at resonant wavelengths of 1.3237 and 1.3457 and 1.3982 and 1.4306 μm).

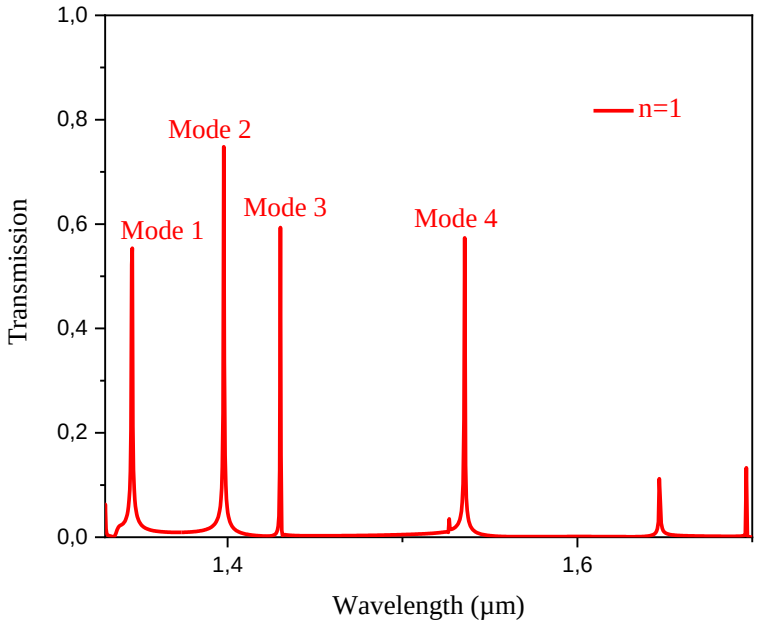

Figure III-15: The normalized transmission spectrum for n=1.

III-6-2 Optimization of the proposed design

We now turn our attention to the optimization of the PhC design since the structure optimizations can further improve the performance. The optimization is performed by changing three parameters, the capsule length E, the capsule radius RE and the radius of specific holes R_c, by properly arranging R_c, E and RE, it is possible to improve the performance of our PhC biosensor.

We propose a step-by-step optimization procedure for the proposed PhC biosensor and the proposed optimization approach is presented in figure III-16. All possible geometry parameters are optimized, and our results reveal the relationship between geometrical parameters and the performance of the capsule-shaped biosensor. The final optimized parameters for the new PhC device are R_c =0.19a µm, E= 0.46 µm, and RE=0.47 µm, respectively.

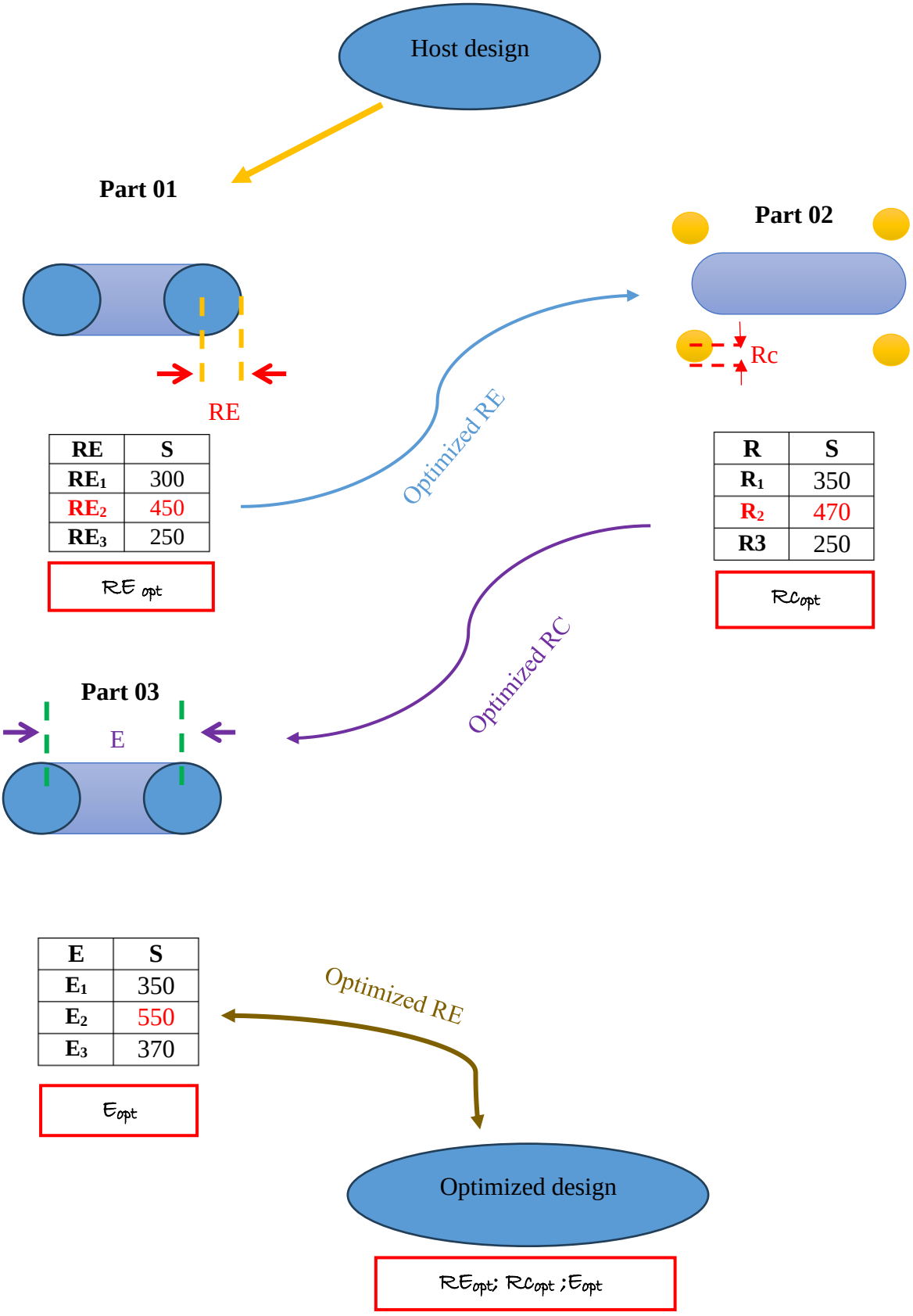

RE	S
RE_1	300
RE_2	450
RE_3	250

R	S
R_1	350
R_2	470
R3	250

E	S
E_1	350
E_2	550
E_3	370

Figure III-16: Optimization of the proposed design.

III-6-2-1 Optimization of the capsule radius (RE)

In order to maximize the sensitivity of the suggested design, we are currently concentrating on optimizing the capsule radius (RE) for (n=1.33 and n=1.332) to achieve the best sensitivity. We focus on just two modes (modes 3 and 4); since the transmission is optimal. As we can see clearly in Table III-3 and Figure III.17, the best value of the capsule radius RE is 0.47µm which corresponds to the highest sensitivity (709.5nm/RIU).

Table III-3 : Optimization of the capsule radius (RE) for modes 3 and 4.

RE (µm)	λ_{res} (µm) (n=1.33)		λ_{res} (µm) (n=1.332)		S(nm/RIU)	
	Mode 3	Mode 4	Mode 3	Mode 4	Mode 3	Mode 4
0.45	1.700102	1.734004	1.700970	1.735207	434	601.5
0.46	1.672241	1.709110	1.673080	1.710279	419.5	584.5
0.47	1.644466	1.683785	1.645549	1.685204	541.5	709.5
0.48	1.613684	1.656452	1.614466	1.657825	391	686.5
0.49	1.580778	1.622850	1.581778	1.624168	500	659

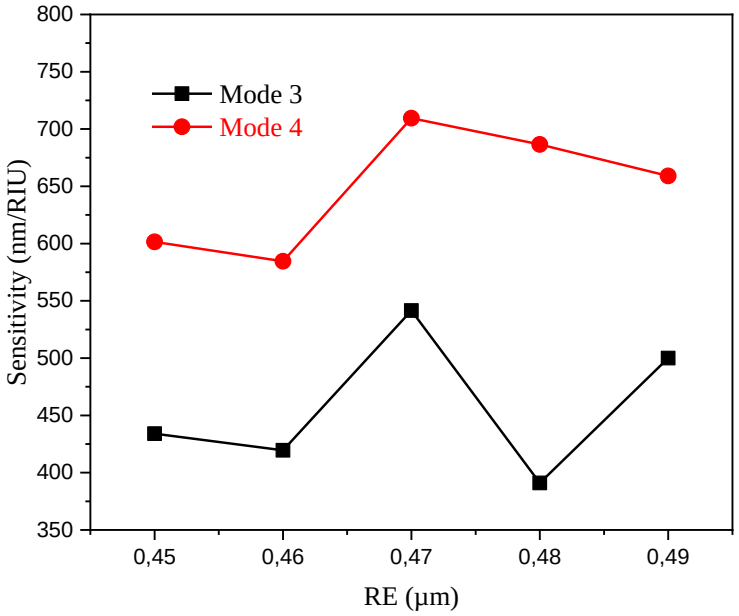

Figure III-17: Effect of capsule radius (RE) on the sensitivity of the suggested design.

III-6-2-2 Optimization of the radius of the holes surrounding the capsule- shaped cavity (R_c)

Now, we turn our attention to the optimization of the radius of the holes surrounding the capsule-shaped cavity (R_c) of the proposed design for (n=1.33 and n=1.332) to achieve the best sensitivity. We have changed the value of R_c from 0.16a µm to 0.26a µm with a step of 0.1µm and we have found that the best value of the radius of holes surrounding the capsule-shaped cavity (R_c) is 0.19a µm, which corresponds to the highest sensitivity (727nm/RIU), as Table III-5 and Figure III.18 clearly show.

Table III-4: Optimization of the radius of the holes surrounding the capsule- shaped cavity (R_c).

	λ_{res} (µm) (n=1.33)		λ_{res} (µm) (n=1.332)		S(nm/RIU)	
Rc (µm)	**Mode 3**	**Mode 4**	**Mode 3**	**Mode 4**	**Mode 3**	**Mode 4**
0.16a	1.653166	1.713796	1.653986	1.714971	410	587.5
0.17a	1.652619	1.710864	1.653439	1.712036	410	586
0.18a	1.6518	1.707942	1.652619	1.70911	409.5	584
0.19a	1.650982	1.704739	1.652073	1.706193	545.5	727
0.20a	1.650165	1.701838	1.651255	1.703287	545	724.5
0.21a	1.649349	1.698658	1.650165	1.700102	408	722
0.22a	1.648261	1.695203	1.649349	1.696641	544	719

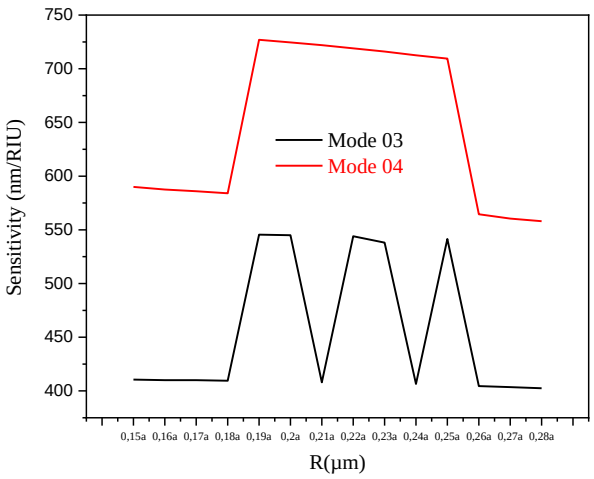

Figure III-18: Effect of the radius of the holes surrounding the capsule-shaped cavity (R) on the sensitivity of the suggested design.

III-6-2-3 Optimization of the capsule length (E)

The last parameter to optimize in order to maximize the sensitivity for (n=1.33 and n=1.332) of the proposed design is the capsule length (E). The value of E is changed from 0.44 µm to 0.48 µm with a step of 0.1µm and the obtained results are shown in Table III-7 and Figure III-19. It is evident from this figure that E=0.45µm is the best value of capsule length (E) which corresponds to a sensitivity of 734nm/RIU.

Table III-5 : Optimization of the capsule length (E).

E (µm)	λ_{res} (µm) (n=1.33)		λ_{res} (µm) (n=1.332)		S(nm/RIU)	
	Mode 3	**Mode 4**	**Mode 3**	**Mode 4**	**Mode 3**	**Mode 4**
0.44	1.659476	1.716444	1.660299	1.717623	411.5	589.5
0.45	1.656726	1.712622	1.65755	1.71409	412	734
0.46	1.653713	1.708817	1.654807	1.710279	547	731
0.47	1.650982	1.704739	1.652073	1.706193	545.5	727
0.48	1.648261	1.70068	1.649077	1.701838	408	579

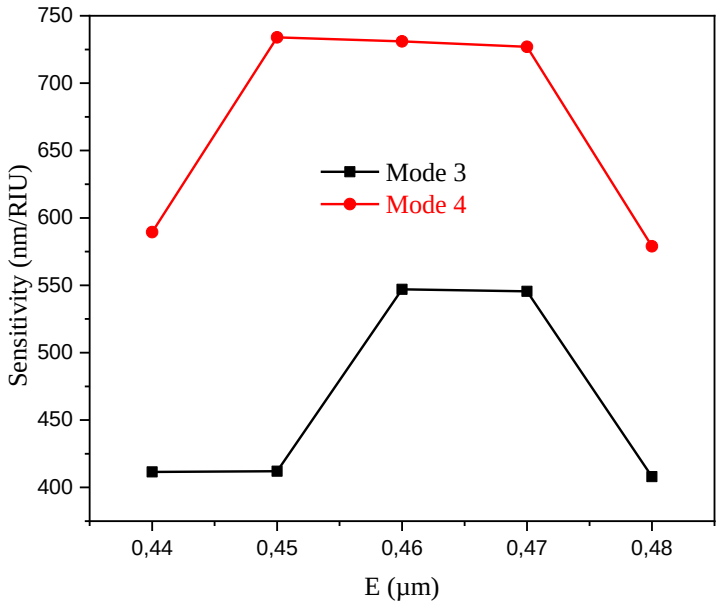

Figure III-19: Effect of capsule length (E) on the sensitivity of the proposed design.

The performance of the capsule-shaped biosensor depends on several geometrical parameters which are: lattice constant and air holes radius of the structure (R_c), capsule radius (RE) and length (E), and finally, the radius of the holes surrounding the capsule-shaped cavity (R). A sketch of the geometry highlighting these different parameters is shown in Figure III-18. To enhance the performance the suggested biosensor and maximize its sensitivity, its geometrical parameters shown in Figure III-20 have been studied and analyzed. It was found that the best optimized geometrical parameters of the structure.

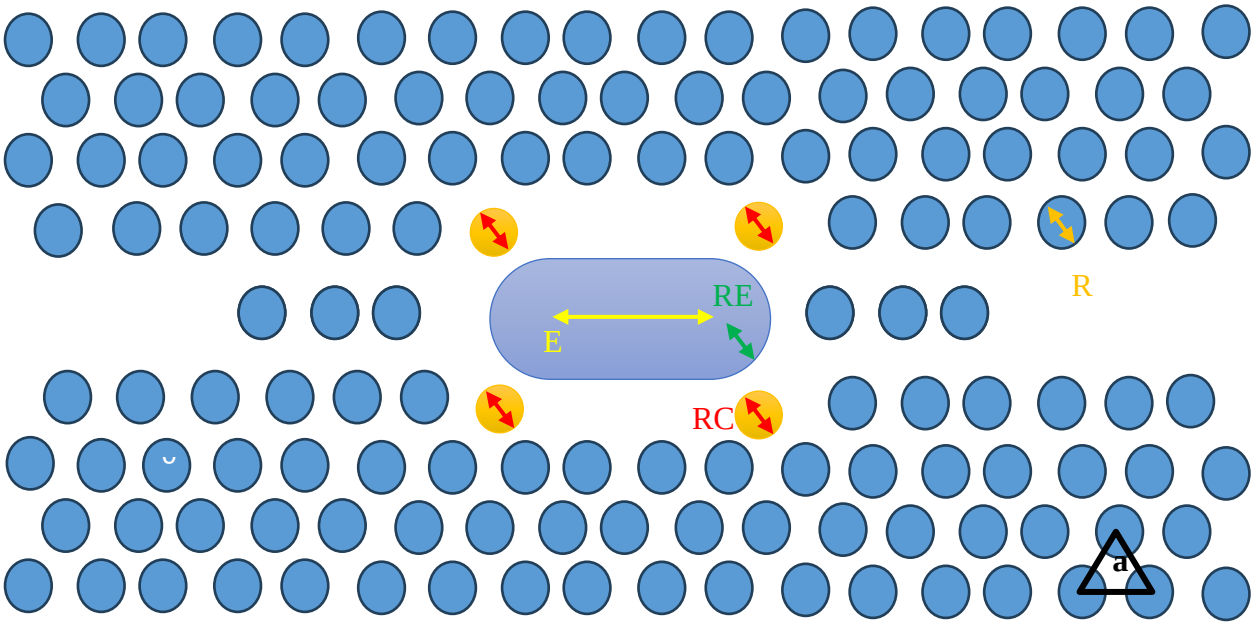

Figure III-20: The optimized parameters are: E, RE, and R_c.

III-7 Application of the proposed design for detecting brain tumors

Brain cancers are the second most prevalent type of cancer, making up around 15% of all cancers [54]. The brain regulates impulses, muscles, organs, blood vessels, smell, taste, hearing, vision, and touch, among other functions (Figure III-21). As a result, the way symptoms manifest differs depending on these functions.

Treating brain cancers, including non-malignant brain tumors, presents greater complexity compared to the management of some other cancer types. Surgical removal of the tumor is not always feasible due to either its inaccessibility or the risk of damaging critical brain regions during the procedure [55]. Inoperable brain areas encompass the brain stem, thalamus, motor cortex, and deep gray matter regions. The prognosis of a brain tumor depends not only on its type, grade, and size, but also on its specific location within the brain [54].

Male brain tumors pose additional challenges in treatment [55]. The **blood-brain barrier acts as a formidable obstacle, preventing systemic chemotherapy from effectively**

reaching the tumor within the brain. This barrier restricts the passage of therapeutic agents, making treatment more complex. Understanding brain cancers and their unique characteristics is crucial for devising effective treatment strategies and improving patient outcomes.

In this context, a 2D photonic crystal sensor is proposed to identify different types of brain cancer, aiming to achieve the highest sensitivity and accuracy in analysis. Utilizing photonic crystals in this manner represents an innovative approach, enabling a deeper understanding of tumor characteristics and a more precise identification of their type. This technology holds the potential to enhance treatment by enabling more targeted approaches, thereby improving the prospects for recovery and outcomes for patients with brain cancer [54].

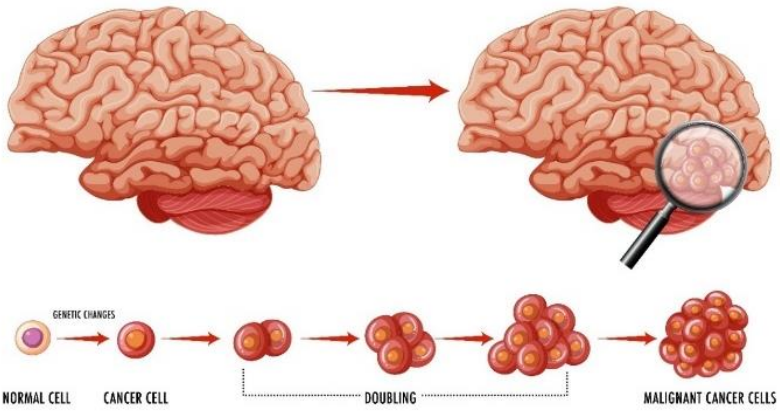

Figure III-21: Cancer development process.

III-7-1 Type of cancer brain

A- Medulloblastomas

Medulloblastomas arise from primitive neuroectodermal tissue (PNET). PNET encompasses a wide range of brain tumors originating from immature brain cells. These highly malignant tumors typically manifest in the cerebellum. They exhibit rapid growth and often utilize the cerebrospinal fluid to spread to other regions within the central nervous system. Medulloblastomas are particularly prevalent in pediatric cases [56].

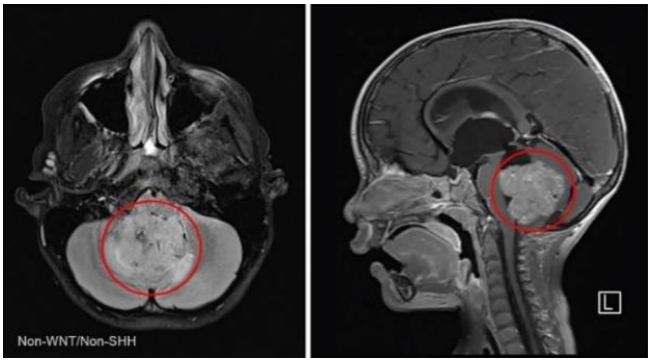

Figure III-22: Radio X cancer type Medulloblastomas [57].

B- Glioblastoma

Glioblastoma, also known as glioblastoma multiforme (GBM), belongs to the category of astrocytomas, which are malignant brain tumors. The broader group of brain tumors called gliomas encompasses both glioblastomas and astrocytomas [58].

Astrocytes, star-shaped cells, serve as the origin for both glioblastomas and astrocytomas. However, within a GBM tumor, one may also encounter malignant blood vessels and areas containing dead cells [59].

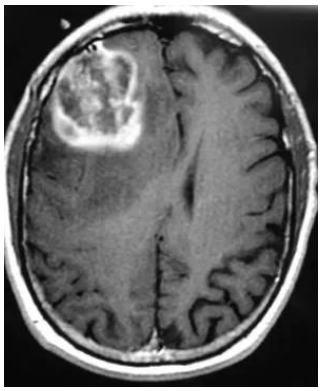

Figure III-23: Radio X cancer type Glioblastoma [60].

C- Lymphoma

Brain lymphoma, also referred to as primary cerebral lymphoma or primary central nervous system lymphoma (PCNSL), is a rare and highly aggressive subtype of non-Hodgkin lymphoma. It originates in the lymph tissue (white blood cells) within the brain, spinal cord, and cerebrospinal fluid (CSF). In some cases, it can also affect the eyes. Early detection is crucial, as this type of cancer can be effectively treated and even cured if identified promptly [61].

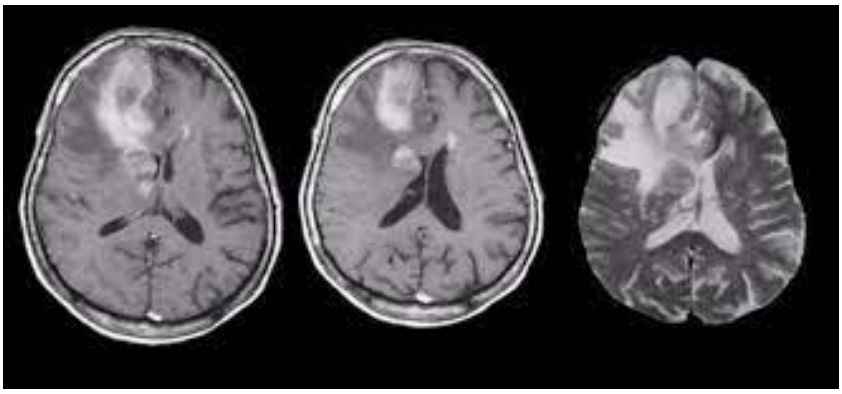

Figure III-24: Radio X cancer type lymphoma [62].

D- Metastases

Brain metastases occur when cancer cells spread from their original site to the brain. While any type of cancer can potentially spread to the brain, certain cancers are more likely to cause brain metastases. These include lung, breast, colon, kidney, and melanoma cancers.

Brain metastases can manifest as single tumors or multiple tumors within the brain. As these metastatic brain tumors grow, they exert pressure on and alter the function of surrounding brain tissue. Consequently, individuals may experience various signs and symptoms, such as [63]:

→ **Headache**, sometimes accompanied by vomiting or nausea.
→ **Mental changes**, including increasing memory problems.
→ **Seizures**.
→ **Weakness or numbness** on one side of the body.

Early detection is crucial, as timely intervention can lead to effective treatment and improved outcomes. Treatment options for brain metastases may include surgery, radiation therapy, chemotherapy, immunotherapy, or a combination of approaches. Additionally, managing pain and symptoms resulting from cancer is an essential aspect of care [58].

Brain metastases occur when cancer cells spread from their original site to the brain. Any cancer can spread to the brain, but the types most likely to cause brain metastases are lung, breast, colon, kidney, and melanoma [59].

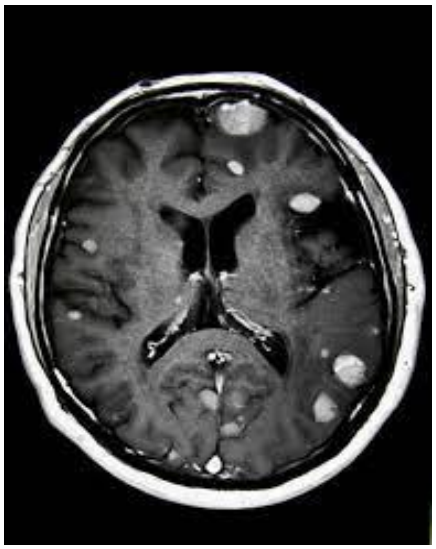

Figure III-25: Radio X cancer type lymphoma [64].

III-7-2 The proposed sensor's design

This section will primarily focus on the design, simulation, and testing of the proposed sensor design. This section will be divided into two main subsections. The first portion covers the basic design. Section two discusses the revised design. The design stages are separated to provide a comprehensive understanding of the analysis, testing, and assessment process. Another goal is to create all of the testing and optimization processes that must be carried out. Analyzing the results of these processes and trials will help define the appropriate performance values or properties with regard to the major assessment parameters, simplicity, quality factor, sensitivity, and detection limit.

Before entering the design stage, it's important to state that the sensor's design stages will depend mainly on the accurate measurement of the refractive index (RI) for several brain tissues. represents the RI of several brain tissues and will be used to indicate the situation of the sample if it's normal or abnormal status. Each accurate refractive index measurement will be associated with a type of normal or abnormal tissue, as indicated in Table III-9.

Table III-6 : The refractive index of several types of brain tissues [65].

	Tissue	Physical Density gm/cm^3	Water	RI Mean
CSF	**Cerebrospinal fluid**	1.000	100	1.3333
Normal tissues	**Gray matter**	1.034	99	1.3951
	White matter	1.029	97.5	1.4121
Abnormal tissues	**Wall of solid drain abscess**	1.028	97	1.3412
	Multiple sclerosis	1.031	96	1.3425
	Oligodendroglioma	1.056	94	1.3531
	Low grade glioma	1.206	58	1.4320
	Medulloblastoma	1.318	53	1.4412
	Glioblastoma	1.343	49	1.4470
	Lymphoma	1.378	42	1.4591
	Metastasis	1.423	29	1.4833

III-7-3 Design of a RI Biosensor for Brain Cancer

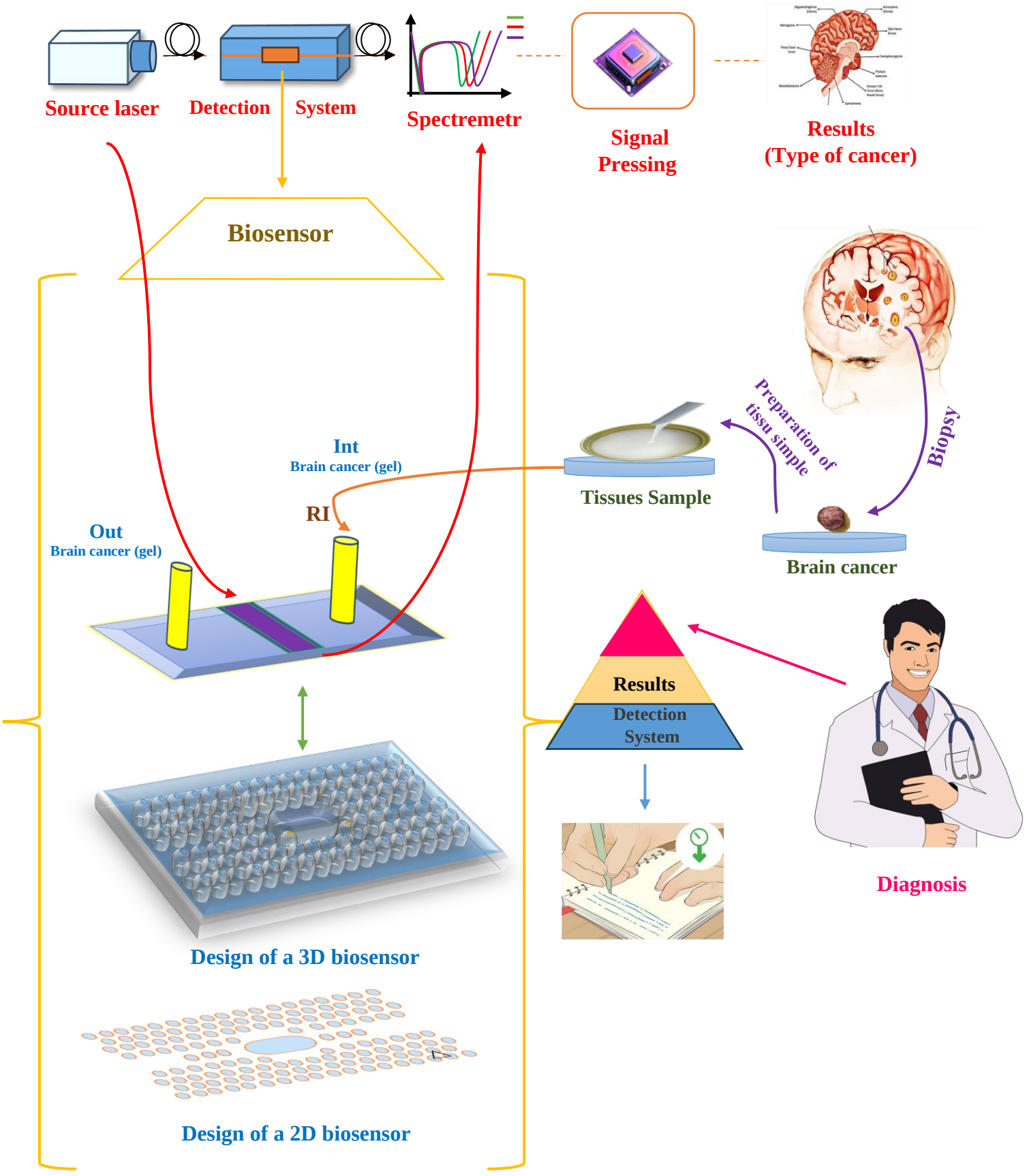

Figure III-26: Detection system of Brain Cancer based on PhCs RI Biosensor

III-7-4 Results and discussion

The design, simulation, and testing of the suggested sensor will be the main focus of this section. There will be two primary subsections in this section. The optimized design is covered in the first section of normally tissue. The optimized design is covered sick tissue in section two. To give a thorough understanding of the analysis, testing, and assessment process, the design stages are divided. Creating the numerous optimization procedures and experiments that are need to be conducted is another objective.

To determine the ideal performance values or property with respect to the four primary assessment parameters—FOM, quality factor, sensitivity, and detection limit—the outcomes of these procedures and experiments will be utilized.

Another key feature of interest in this work is to differentiate between normal and cancer cell lines by infiltrating different sample cells into the structure. Here, we introduced both the normal and cancerous brain tissues as an analyte. The human brain floats in a colorless fluid called Cerebrospinal fluid (CSF). Since it is a well-established fact that the refractive index of CSF of a healthy person is 1.3333, we will take this value of the refractive index as an internal reference to carry out the findings of the proposed work [66].

III-7-4-1 Results and discussion of normal tissues

Gray matter constitutes a significant part of the central nervous system. It comprises neuronal cell bodies, as well as other cells like glia and dendrites. These regions are involved in processing information, decision-making, and memory. In essence, gray matter is where the computational work of the brain occurs [60].

White matter consists of bundles of myelinated axons (nerve fibers). Unlike gray matter, it contains few cell bodies. White matter serves as the communication network, connecting various gray matter regions. The myelin sheath around axons facilitates rapid transmission of nerve signals [59].

To describe the sensor's efficiency the following parameters must be introduced:

- **Wavelength**: It is the wavelength of the light being used. It's measured in micrometers (μm).
- **FWHM**: It0 0could be a specific parameter related to the mode of light propagation, but without additional context, it's hard to provide a precise definition.
- **Q-factor**: It is a dimensionless parameter that describes how underdamped an oscillator or resonator is. It represents the bandwidth relative to its center frequency. Higher Q indicates a lower rate of energy loss and the oscillations die out more slowly.

- **Sensitivity (nm/RIU)**: Represents the sensitivity of the system to changes in the refractive index. It's measured in nanometers per Refractive Index Unit (RIU). A higher value means the system is more sensitive to changes in the refractive index.
- **FOM (RIU^{-1})**: It is the Figure of Merit, a measure of the system's performance. It's calculated as the sensitivity divided by the full width at half maximum (FWHM), hence the units of RIU^{-1}. A higher FOM indicates better performance.

  DL (RIU): It could be the detection limit of the system, measured in RIU. A lower detection limit means the system can detect smaller changes in the refractive index.

Table III-10 summarizes the optical properties of different brain tissues, including cerebrospinal fluid (CSF), gray matter, and white matter. The parameters such as wavelength, Q-factor, sensitivity, and figure of merit (FOM) are essential for understanding light interactions within the brain.

Table III-7: The values of resonant wavelength, Q-factor, sensitivity, FOM, and DL of normal brain tissues (Gray and white matter) for modes 3 and 4.

	Brain Tissues	Wavelength (µm)	FWHM	Q-Factor	Sensitivity (nm/RIU)	FOM (RIU^{-1})	DL (RIU)
	CSF (n=1.333)	1.655355	X	X	X	X	X
Mode 3	Gray matter (n=1.3951)	1.683218	3.59×10^{-4}	4.71×10^{6}	579.83	1.61×10^{6}	6.19×10^{-8}
Mode 3	White matter (n=1.4121)	1.691189	2.51×10^{-4}	6.73×10^{6}	454.74	1.81×10^{6}	5.52×10^{-7}
Mode 4	Gray matter (n=1.3951)	1.752541	7.85×10^{-4}	2.23×10^{6}	669.64	8.54×10^{5}	1.17×10^{-7}
Mode 4	White matter (n=1.4121)	1.763668	4.43×10^{-4}	3.98×10^{6}	666.38	1.50×10^{6}	6.65×10^{-7}

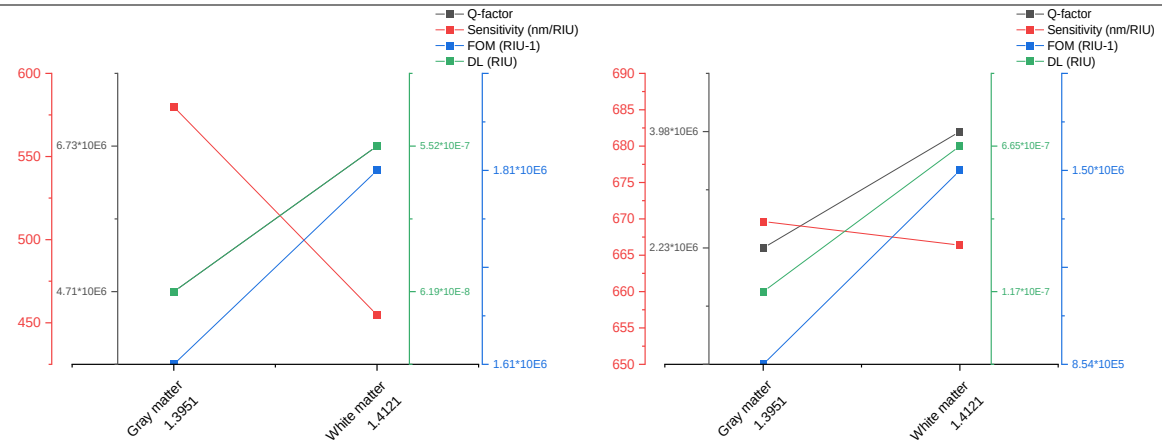

(a) (b)

Figure III-27: FOM, quality factor, sensitivity, and detection limit of mode three (a) and mode four (b).

For each tissue type (CSF, gray matter, and white matter), different modes (03 and 04) are being analyzed. Each mode has a different set of parameters, indicating how light of a specific wavelength propagates through that particular tissue. The exact interpretation of these values would depend on the specifics of the system and the context in which these measurements were taken.

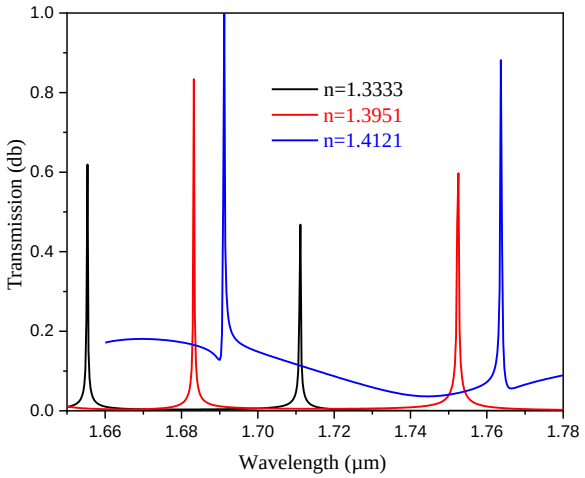

Figure III-28: The normalized transmission spectra of normal brain tissues (Gray and white matter) for modes 3 and 4.

III-7-4-2 Results and discussion of abnormal tissues

The propagation of light through abnormal or diseased brain tissues, such as those found in brain cancer, can be significantly different from its propagation through healthy tissues. This is due to changes in the optical properties of the tissues, which can be affected by various factors including changes in tissue composition, structure, and blood supply [64]..

In the context of brain cancer, these changes can include an increase in cell density, changes in the structure of the extracellular matrix, and alterations in the blood vessels supplying the tumor. These changes can affect the absorption and scattering of light, which in turn can affect the propagation of light through the tissue [62].

In the case of brain cancer, these optical imaging techniques could potentially provide valuable information about the tumor, such as its size, location, and the extent of its infiltration into the surrounding brain tissue [59]. However, the accuracy and reliability of these techniques depend on the accuracy of the light propagation models used, and on the specific optical properties of the abnormal brain tissue. It’s important to note that while these techniques show promise, they are still under investigation and are not yet widely used in clinical practice for the detection or diagnosis of brain cancer[48].

III-7-4-2-1 Results and discussion of abnormal tissues for mode three

The utilization of photonic crystals for the meticulous examination of brain tissues represents a promising frontier in medical diagnostics and research, including the detection of brain cancer. By harnessing parameters like resonant wavelength, Q-factor, sensitivity, figure of merit (FOM), and detection limit (DL), there's a profound opportunity to engineer biosensors that are not only highly sensitive but also compact, facilitating the early detection of brain lesions, including cancerous growths. This intricate interplay of parameters underscores the potential to revolutionize our approach to diagnosing neurological disorders, paving the way for more effective treatments and improved patient outcomes. In the subsequent section, we delve deeper into the intricacies of mode three's optimized design, exploring how these parameters can be finely tuned to enhance sensor performance and reliability in detecting minute abnormalities within brain tissues.

Table III-8 : The values of resonant wavelength, Q-factor, sensitivity, FOM, and DL of abnormal brain tissues for mode 3.

Brain Tissues	Wavelength (µm)	FWHM	Q-factor	Sensitivity (nm/RIU)	FOM (RIU^{-1})	DL (RIU)
CSF (n=1.333)	1.655355	X	X	X	X	X
Wall of solid Darin abscess (n=1.341)	1.658925	5.72×10^{-4}	2.90×10^{6}	451.90	7.90×10^{5}	1.27×10^{-7}
Multiple sclerosis (n=1.343)	1.659476	4.82×10^{-4}	3.44×10^{6}	447.93	9.29×10^{5}	1.08×10^{-7}
Oligodendroglioma (n=1.35)	1.664170	3.74×10^{-4}	4.46×10^{6}	445.20	1.19×10^{6}	8.39×10^{-8}
Low grade glioma (n=1.432)	1.700391	4.43×10^{-4}	3.84×10^{6}	456.29	1.03×10^{6}	9.71×10^{-8}
Medulloblastoma (n=1.441)	1.704733	5.24×10^{-4}	3.25×10^{6}	457.64	8.73×10^{5}	1.15×10^{-7}
Glioblastoma (n=1.447)	1.707359	4.51×10^{-4}	3.78×10^{6}	457.38	1.01×10^{6}	9.87×10^{-8}
Lymphoma (n=1.459)	1.713209	6.92×10^{-4}	2.47×10^{6}	459.89	6.64×10^{5}	1.51×10^{-7}
Metastasis (n=1.483)	1.724733	7.40×10^{-4}	2.33×10^{6}	462.52	6.25×10^{5}	1.60×10^{-7}

It’s clear from Figure III-29 that for:

- **Wall of Solid Brain Abscess**: The curve for the wall of a solid brain abscess shows a gradual increase in the Q-factor as the wavelength increases. Sensitivity remains relatively constant, indicating that this tissue responds consistently to changes in wavelength.

- **Multiple Sclerosis**: The curve for multiple sclerosis exhibits a similar trend, with a slight increase in both Q-factor and sensitivity. The FOM (Figure of Merit) remains relatively stable.
- **Oligodendroglioma**: Oligodendroglioma's curve shows a steeper rise in Q-factor and sensitivity. The FOM continues to improve, suggesting that this tissue is highly responsive within the measured range.
- **Low-Grade Glioma**: The curve for low-grade glioma displays a peak in sensitivity around 1.432 µm. Both Q-factor and FOM remain favorable.
- **Medulloblastoma**: Medulloblastoma's curve is characterized by a broad peak in sensitivity around 1.441 µm. The Q-factor remains high, indicating efficient interaction with light.
- **Glioblastoma**: Glioblastoma's curve resembles a plateau, with consistent Q-factor and sensitivity. The FOM remains adequate.
- **Lymphoma**: Lymphoma's curve shows a gradual decline in sensitivity as the wavelength increases. The Q-factor remains relatively stable.
- **Metastasis**: Metastasis exhibits a similar trend to lymphoma, with a slight decrease in sensitivity. The FOM remains reasonable.

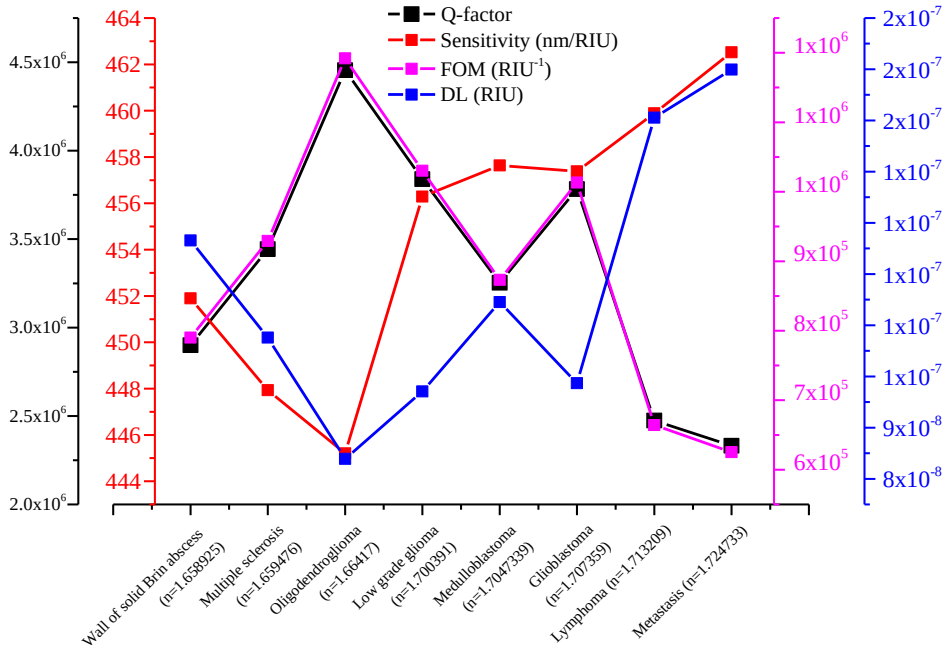

Figure III-29: Resonant wavelength, Q-factor, sensitivity, FOM, and DL of abnormal brain tissues for mode 3.

Different abnormal brain tissues are listed along with their refractive indices (n) and corresponding transmission spectra. These tissues include gliomas (such as oligodendroglioma, low-grade glioma, medulloblastoma, and glioblastoma), lymphoma, metastasis, and others.

Despite variations in refractive indices and tissue types, many tissues exhibit similar transmission spectra, with transmission values clustered around 1. understanding transmission spectra of abnormal brain tissues can provide vital information for disease diagnosis, assessment, and treatment guidance, thereby improving patient care and advancing medical therapies.

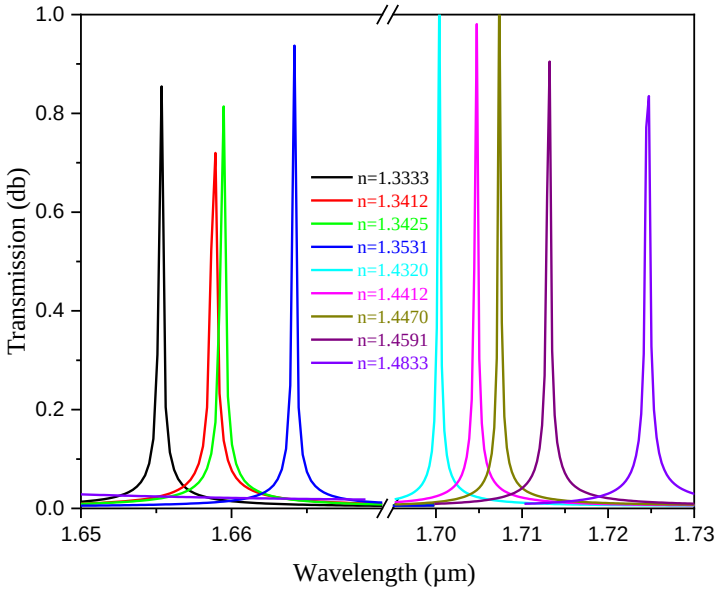

Figure III-30: The normalized transmission spectra of abnormal brain tissues for mode 3.

III-7-4-2-2 Results and discussion of abnormal tissues for mode four

The ability to precisely analyze brain tissues using photonic crystals holds great promise for medical diagnostics and research. Resonant wavelength, Q-factor, sensitivity, FOM, and DL, are essential for developing highly sensitive and compact biosensors that can detect brain lesions early on. The subsequent section addresses the optimized design of mode four.

Table III-09 : The values of resonant wavelength, Q-factor, sensitivity, FOM, and DL of abnormal brain tissues for mode 4.

Brain Tissues	Wavelength (μm)	FWHM	Q-factor	Sensitivity (nm/RIU)	FOM (RIU^{-1})	DL (RIU)
CSF (n=1.333)	1.711157	X	X	X	X	X
Wall of solid Darin abscess (n=1.341)	1.716444	4.75×10^{-4}	3.62×10^{6}	669.24	1.41×10^{6}	7.09×10^{-8}
Multiple sclerosis (n=1.343)	1.717328	6.28×10^{-4}	2.73×10^{6}	670.76	1.07×10^{6}	9.37×10^{-8}
Oligodendroglioma (n=1.353)	1.724435	7.04×10^{-4}	2.45×10^{6}	670.61	9.52×10^{5}	1.05×10^{-7}
Low grade glioma (n=1.432)	1.77683	8.64×10^{-4}	2.06×10^{6}	665.38	7.70×10^{5}	1.30×10^{-7}
Medulloblastoma (n=1.441)	1.783167	8.06×10^{-4}	2.21×10^{6}	667.38	8.28×10^{5}	1.21×10^{-7}
Glioblastoma (n=1.447)	1.783167	8.27×10^{-4}	2.16×10^{6}	633.33	7.66×10^{5}	1.31×10^{-7}
Lymphoma (n=1.459)	1.79501	8.94×10^{-4}	2.01×10^{6}	666.56	7.46×10^{5}	1.34×10^{-7}
Metastasis (n=1.483)	1.81061	9.85×10^{-4}	1.84×10^{6}	663.02	6.73×10^{5}	1.49×10^{-7}

It's clear from Figure III-31 that for:

- **Wall of Solid Brain Abscess:** The Q-factor increases as the wavelength approaches 1.341 μm, creating a peak. The sensitivity, FOM, and DL also exhibit a peak around this wavelength, indicating optimal performance for detecting brain abscesses.
- **Multiple Sclerosis:** The sensitivity, FOM, and DL show a similar peak around 1.343 μm, suggesting good diagnostic capabilities. However, the Q-factor remains relatively constant.
- **Oligodendroglioma**: The Q-factor increases slightly, but the sensitivity, FOM, and DL remain stable. This tissue behaves consistently across the measured wavelengths.
- **Low-Grade Glioma:** The Q-factor shows a gradual increase, while the sensitivity, FOM, and DL remain steady. This tissue exhibits moderate optical properties.
- **Medulloblastoma:** The Q-factor and sensitivity both peak around 1.441 μm, indicating optimal performance. The FOM and DL remain relatively constant.
- **Glioblastoma:** The Q-factor decreases significantly, suggesting less efficient optical behavior. The sensitivity, FOM, and DL also decrease, indicating challenges in detection.

- **Lymphoma:** The Q-factor remains stable, but the sensitivity, FOM, and DL show a slight dip. Lymphoma tissue may be less responsive to optical measurements.
- **Metastasis:** The Q-factor decreases further, indicating poor optical behavior. The sensitivity, FOM, and DL also decrease significantly. Detecting metastatic tissue using these properties may be challenging.

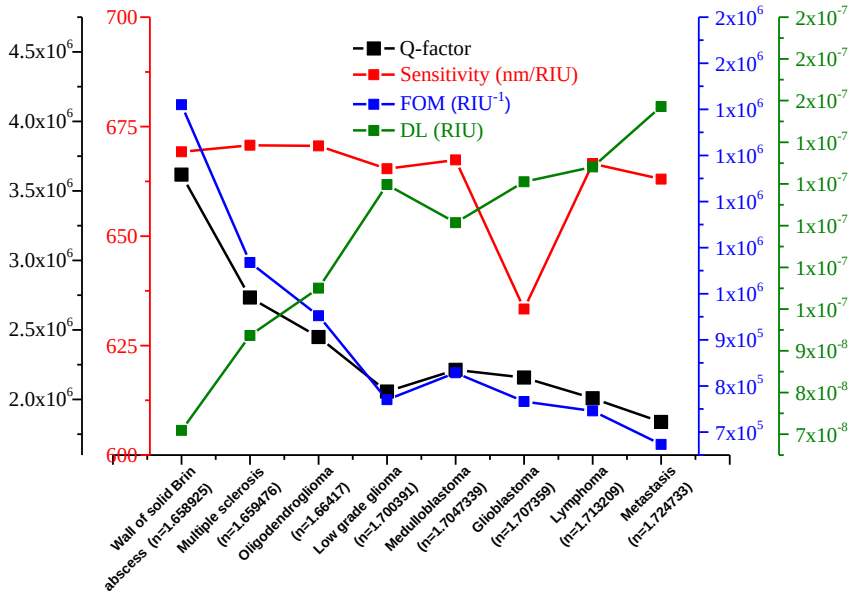

Figure III-31: The normalized transmission spectra of abnormal brain tissues for mode 4.

In summary, the brain tissues exhibit diverse optical responses, with some showing distinct peaks and others maintaining consistent behavior. These curves provide valuable insights for medical diagnostics and research.

Figure III-32 shows the transmission spectrum of the biosensor by changing the refractive index of brain cancer. The resonant wavelength is shifted to the longer wavelengths by increasing the refractive index.

Given that the spectral behavior of transmission depends on several factors, including the characteristics of the tissues and diseases under study, its effectiveness varies depending on the specific context. In medical contexts, transmission can identify cancerous tumors in their early stages or differentiate between different types of brain tumors.

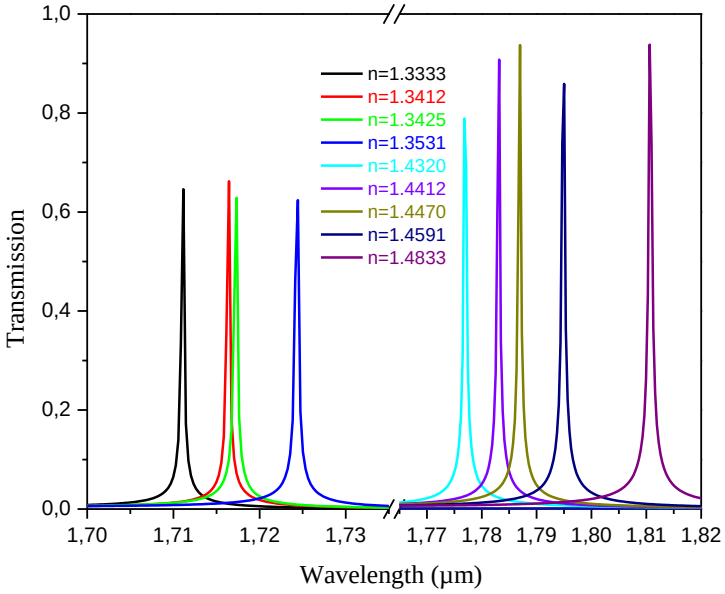

Figure III-32: The normalized transmission spectra of abnormal brain tissues for mode 4.

III-8 Application of the proposed design for detecting covid-19

The beginning of the novel coronavirus (COVID-19) pandemic dates back to December 2019 when initial cases of an unidentified pneumonia were reported in Wuhan, Hubei Province, China. In the following months, the virus spread rapidly around the world, leading the World Health Organization (WHO) to declare on March 11, 2020 that the epidemic had become a global pandemic. Since then, cases of infection with the virus have been recorded in most countries of the world, and preventive and precautionary measures have been taken to limit its spread and reduce the negative health and economic impact of the epidemic.

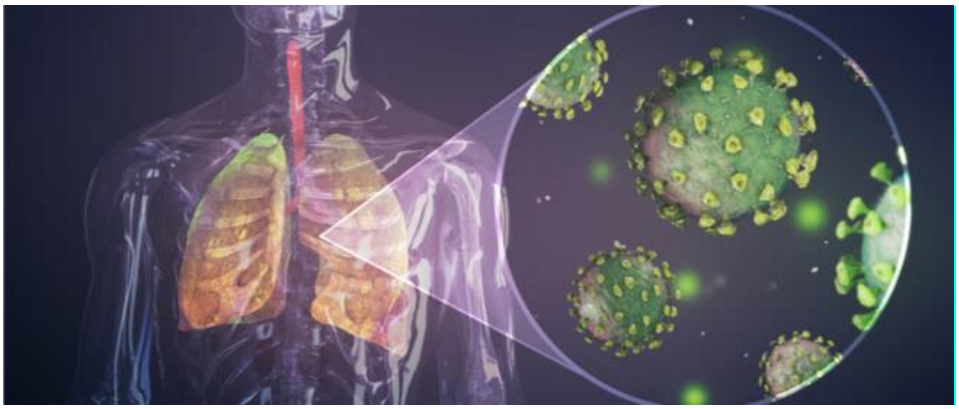

Figure III-33: Development of coronavirus.

Deep tissue testing (PCR) test is the main method for diagnosing COVID-19. Genetic material is collected from the nose or throat using a swab and then analyzed in a laboratory for the presence of the virus.

This part was added to obtain the patent for the development of biosensors for Covid-19 discovery.

III-8-1 Refractive index of Antibody compounds covid-19 (IGg, IGm)

Before entering the design stage, it's important to state that the sensor's design stages will depend mainly on the accurate measurement of the refractive index (RI) of Antibody compounds covid-19 (IGg, IGm) and the normal blood, as indicated in Table III-9.

Table III-10: The refractive index of Antibody compounds covid-19 [67].

Compounds	RI
Blood	1.3
Igg	1.3448
IGm	1.3493

III-8-2 Results and discussion of covid-19

The detection of IgG and IgM antibodies related to Covid-19 using photonic crystals relies on the principle of changes in the refractive index of the surrounding medium due to the presence of these antibodies. The photonic crystal structure is designed to be highly sensitive to small variations in the refractive index, where such changes lead to a significant shift in the resonant wavelength of the structure [68.69].

When the photonic crystal structure is exposed to a liquid sample, such as plasma or serum, containing IgG or IgM antibodies specific to Covid-19, these antibodies will interact with the sensitive surface of the structure and slightly alter the refractive index of the surrounding medium. This small change in the refractive index will result in a noticeable shift in the resonant wavelength of the photonic crystal structure, which can be accurately measured using techniques like spectral analysis [68.69].

Because of the high sensitivity, excellent resonance sharpness, and low detection limits of photonic crystal structures, the presence of IgG and IgM antibodies related to Covid-19 can be detected with high accuracy, even at very low concentrations. This makes photonic crystals a powerful tool for early detection of Covid-19 infection and evaluating the immune system's response to the virus. [70].

The high sensitivity enables the photonic crystal structure to detect minute changes in the refractive index caused by the binding of IgG or IgM antibodies to the sensor surface. The sharp resonances and high Q-factors allow for precise measurement of the resonant wavelength shift, while the low detection limits ensure that even trace amounts of antibodies can be reliably detected.

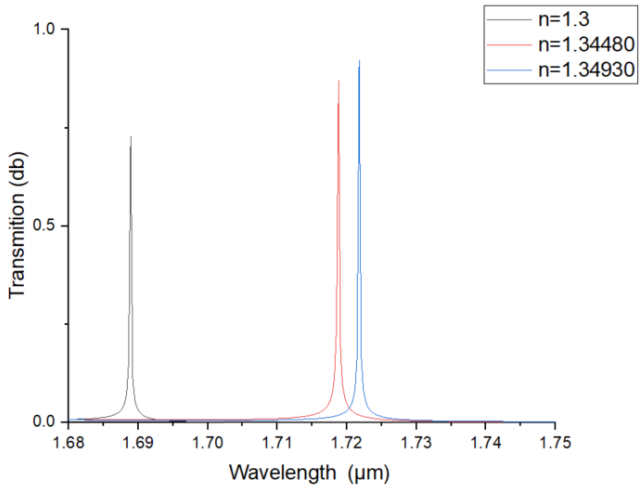

Figure III-34: The normalized transmission spectra of covid 19.

the displayed values indicate good performance of the photonic crystal structure as a biosensor. Here are some observations on the values. The refractive index (RI) values range between 1.3 and 1.3493, which are reasonable values for plastic or glass materials that can be used in fabricating the photonic crystal structure. The full-width at half-maximum (WHFM) values are very small (2.51×10^{-4} and 3.59×10^{-4}), indicating high sharpness of the resonance peaks or bands of the structure, which is desirable for improving detection capability. The Q-factor values are extremely high (6.86×10^{6} and 4.79×10^{6}), meaning high sharpness of the resonance peaks and better performance for sensing. The sensitivity values (667.4 and 666.5 nm/RIU) are reasonably high, meaning that small changes in the refractive index will lead to a significant shift in the resonant wavelength, facilitating detection. The figure of merit (FOM) values are high (2.65×10^{6} and 1.86×10^{6}), which depend on the sensitivity and full-width at half-

maximum, indicating good overall performance of the structure. The detection limits (DL) are very low (3.77×10^{-8} and 5.38×10^{-8} RIU), meaning the ability to detect extremely small changes in the refractive index.

Table III-11: The values of resonant wavelength, Q-factor, sensitivity, FOM, and DL of covid 19.

RI	Wavelength (µm)	WHFM	Q-factor	Sensitivity (nm/RIU)	FOM (RIU^{-1})	DL (RIU)
1.3	1.688904	X	X	X	X	X
1.3448	1.718804	3.59×10^{-4}	4.79×10^{6}	667.41	1.86×10^{6}	5.38×10^{-8}
1.3493	1.721763	2.51×10^{-4}	6.86×10^{6}	666.51	2.65×10^{6}	3.77×10^{-8}

These values indicate a high-performance photonic crystal structure as a biosensor, with high sensitivity, good resonance sharpness, and a very low detection limit for changes in refractive index. These properties make it suitable for accurately detecting biological molecules and changes in their environment.

III-9 Conclusion

To conclude, we have effectively designed and simulated a novel 2D-PhC platform for the differentiation between normal and abnormal brain tissues, the suggested capsule-shaped biosensor can generate four different modes and it may differentiate between eleven different types of brain lesions, tumors, and cancer tissues. The sensing characteristics of the proposed biosensor are carried out by changing the refractive index of the analyte and our findings have revealed a high sensitivity S=670 nm/RIU, a remarkable Q-factor up to 10^{6}, an ultra-high FOM of 10^{6} RIU^{-1}, and an incredible detection limit of 10^{-8} RIU. Noteworthy to mention that the proposed biosensor can provide a cost-effective and robust approach to diagnosing abnormal brain tissues and the foremost objective of our study to develop a potential alternative to the traditional technique of detecting diseases in the human body with an optical device based on PhC was achieved.

The part of Covid-19 added in order to obtain the patent for the development of biosensors of Covid-19 discovery.

GENERAL CONCLUSION

General conclusion

Photonic crystals are natural or artificial materials whose refractive index varies periodically on the wavelength scale in one, two, or three directions of space, they are new class of materials. Like electrons in semiconductors, photons are distributed in a transmission band separated by a photonic band gap. This analogy allows us to consider the use of photonic crystals to direct light. The development of this new material paves the way for new areas of research and very diverse applications.

The main objective of this master thesis is the design of new structures based on two-dimensional photonic crystals (2D-PhCs) for bio-detection applications operating in the invisible, with the aim of enhancing these sensors' performance.

Firstly, we have presented a general reminder of the fundamental concepts related to photonic crystals and their photonic properties where we have demonstrated the importance of using photonic crystals as a sensor. Then, special emphasis is placed on the study of refraction index (RI) biosensors based on two-dimensional photonic crystals, where the refractive index is set as a parameter to design optical biosensor devices using photonic crystals giving general characteristics and working principles of the different types of sensors and their applications.

In this work, we have successfully designed and simulated a novel 2D-PhC platform for the differentiation between normal and abnormal brain tissues. The suggested capsule-shaped biosensor can generate four different modes and may differentiate between eleven different types of brain lesions, tumors, and cancer tissues using the modules developed by the RSoft-CAD software ideally suited to the design of the 2D photonic circuits, BandSOLVE (based on the PWE method), and FullWAVE (based on the FDTD method), respectively, which are based on direct resolution of Maxwell's equations.

Our results show that the suggested biosensor has a high sensitivity of S=670 nm/RIU, an amazing Q-factor up to 10^6, an ultra-high FOM of 10^6 RIU^{-1}, and an incredible detection limit of 10^{-8} RIU. The sensing features of the biosensor are achieved by varying the refractive index of the analyte. It is noteworthy to mention that the suggested biosensor can offer a cost-effective and robust approach to diagnosing abnormal brain tissues, and our study's primary goal of creating a viable substitute for the conventional method of using an optical device based on PhC to detect diseases in human bodies was accomplished.

In perspective, we encourage PFEs of upcoming promotions, to discover other designs for this sensor and/or to do other processes of optimization such as the layouts and lengths of

the input and output waveguides, to guarantee better coupling between the source and the cavity and also have a better-quality factor.

Part of the Covid-19 for patent. Everything related to this aspect is available in the patent file under number N° : 240457.

References

1. Mohammed, N. A., Khedr, O. E., El-Rabaie, E. M., & Khalaf, A. A. (2023). Brain tumors biomedical sensor with high-quality factor and ultra-compact size based on nanocavity 2D photonic crystal. Alexandria Engineering Journal.
2. Marc ZELSMANN, "Silicon-on-Insulator Photonic Crystals for Light Guiding, Filtering, Emission and Extraction," Doctoral Thesis, Université Joseph Fourier-Grenoble 1, November 2003.
3. E. YABLONOVITCH, Phys. Rev. Lett., 58, 2059-2062 (1987).
4. Yannick MERLE "Study of Electromagnetic Dispersion in Two-Dimensional Periodic Dielectric Materials," Doctoral Thesis No. 47-2003, University of Limoges, November 20, 2003.
5. E. YABLONOVITCH "Photonic Ban-Gap Structure" J. Opt. Society, Vol 10, February 1993.
6. E. YABLONOVITCH, T.J. GMITTER "Photonic Band Structure" J. Opt. Society, Vol 9, September 1990.
7. Benoît LOMBARDET, "Study and Realization of Photonic Crystals for Integrated Optics," Doctoral Thesis No. 3254, Ecole Polytechnique Fédérale de Lausanne (2005).
8. Benaissa Fatima, Study and Simulation of Electromagnetic Wave Propagation in Photonic Crystal Guides-Application to Optical Fibers, Master's in Physics, UNIVERSITY ABOU-BAKR BELKAÏD – TLEMCEN 2012-2013.
9. DEKHIRA Azzeddine, Theoretical Study and Simulation of Photonic Crystals and Their Applications in Chemistry and Biochemistry, MEMOIR, University of Science and Technology Houari Boumediene Faculty of Chemistry, 2010.
10. BEN SALEM Kawthar and SEGHAIRI Imane, Analysis of the Optical Properties of a Highly Nonlinear Microstructured Fiber from its Microscopic Image, Study Memory, Echahid Hamma Lakhdar University of El-Oued Faculty of Technology, 2016-2017.
11. D. Yang, H. Tian and Y. Ji, "The properties of lattice-shifted microcavity in photonic crystal slab and its applications for electro-optical sensor", Sens and Act A: Physical, vol. 171, no. 2.
12. Harhouz, A. Hocini, "Design of high-sensitive biosensor based on cavity waveguides coupling in 2D photonic crystal", Journal of Electromagnetic Waves and Applications, vol. 29, no. 5.

13. B Lombardet. "Study and Realization of Photonic Crystals for Integrated Optics". Doctoral Thesis, École Polytechnique Fédérale de Lausanne. 2005.
14. Maier, S.A. Plasmonics: Fundamentals and Applications; Springer: New York, NY, USA, 2004.
15. M.K. Moghadam, A.R. Attari, M.M. Mirsalehi, Improved photonic crystal directional coupler with short length, Photonics Nanostruct. Fundam. Appl. 8 (2010) pp. 47–53.
16. M.K. Moghadam, A.R. Attari, M.M. Mirsalehi, Improved photonic crystal directional coupler with short length, Photonics Nanostruct. Fundam. Appl. 8 (2010) pp. 47–53.
17. H. Badaoui, M. Feham, M. Abri, Double Bends and Y-Shaped Splitter Design for Integrated Optics, Prog. Electromag. Res. Lett. 28 (2012).
18. Benmerkhi, M. Bouchemat, T. Bouchemat, N. Paraire, Numerical optimization of high Q-factor photonic crystal microcavities with a graded air lattice, J. Opt. Soc. Am. B 28 (2011).
19. Rostami, H.A. Banaei, F. Nazari, A. Bahrami, An ultra-compact photonic crystal wavelength division demultiplexer using resonance cavities in a modified Y-branch structure, Optik 122 (2011).
20. Ghaffari, F. Monifi, M. Djavid, M.S. Abrishamian, Analysis of photonic crystal power splitters with different configurations, J. Appl. Sci. 8 (2008).
21. D. Felbacq, E. Centeno. "Theory of diffraction for 2D photonic crystals with boundary" Optics communications". vol.199.
22. Benmerkhi. "Optimization of Light Confinement in Photonic Crystal Cavities". Doctoral Thesis, Université Mentouri Constantine". 2012.
23. Cohen- Tnouuji, B- Diu. Laloé. "Quantum Mechanics Volume I Hermann". Paris 1973.
24. F. Bougriou "Studies of Two-Dimensional Photonic Crystal Waveguides" Master's Thesis. Université Mentouri Constantine. 2008.
25. M. Grillet. "Photonic Crystals and Photonic Integration". Doctoral Thesis, University of Lyon. 2003.
26. C.J.M. Smith et al. "Coupled guide and cavity in a two-dimensional photonic crystal". Applied Physics Letters. 2001.
27. D.Neel, "Study in Optical Near-Field of Photonic Crystal Waveguides," Doctoral Thesis, Institut National des Sciences Appliquées de Lyon.
28. Deeksha Rani and RS Kaler. Design and Analysis of All Optical Logic Gates Based On 2-D Photonic Crystals. PhD thesis, 2015.

29. Georges Asch, Bernard Poussery "Industrial Instrumentation Sensors 8th Edition", DUNOD 2017.
30. Bougriou Feida, "Theoretical Study of Two-Dimensional Photonic Bandgap Materials: Applications in Optical Waveguiding and Detection," Doctoral Thesis, Université Constantine 1, December 16, 2013.
31. Yacouba Sanogo "Design and Fabrication of Sensors and Their Interrogation Techniques for Applications in Health and Environment," Doctoral Thesis, May 26, 2014.
32. Céline Chouteau. Development of a Bi-Enzymatic Conductimetric Biosensor with Algal Cells. PhD thesis, Lyon, INSA, 2004.
33. Kabir, E.; Uddin, S.M.A.; Chowdhury, S.S. Optimization of Surface Plasmon Resonance Biosensor for Analysis of Lipid Molecules, In Proceedings of the 2020 2nd International Conference on Advanced Information and Communication Technology (ICAICT), Dhaka, Bangladesh, 28–29 November 2020.
34. Sami Laid SAOUCHA. Photonic Crystals for Low-Pressure Sensor Realization. PhD thesis, Université Mohamed Boudiaf-M'sila, 2018.
35. Feida Bougriou. Theoretical Study of Two-Dimensional Photonic Bandgap Materials.
36. Ahlam Harhouz. Contribution to the Study and Design of Photonic Crystal-Based Sensors. PhD thesis, Université de M'sila, 2017.
37. Merzoug Ammari and Farida Hobar. Study of Photonic Crystal-Based Microcavities. PhD thesis. Université de COSTANTEN
38. Shukla, S.K.; Govender, P.P.; Tiwari, A. Polymeric Micellar Structures for Biosensor Technology. In Advances in Biomembranes and Lipid Self-Assembly,1st ed.; Iglic, A., Kulkarni, C.V., Rappolt, M., Eds.; Academic Press: Cambridge, MA, USA, 2016.
39. https://www.nature.com/articles/s41598-022-09213-w.pdf
40. Hossain, M.B.; Tasnim, T.; Abdulrazak, L.F.; Rana, M.M.; Islam, M.R. A Numerical Approach to Design the Kretschmann Configuration Based Refractive Index Graphene-MoS2 Hybrid Layers With TiO2-SiO2 Nano for Formalin Detection. Photonic Sens. 2020.
41. https://link.springer.com/article/10.1007/s12596-023-01524-z
42. https://link.springer.com/article/10.1007/s11082-023-04921-7
43. https://link.springer.com/article/10.1007/s12596-023-01523
44. https://opg.optica.org/josab/abstract.cfm?uri=josab-41-1-222
45. https://ieeexplore.ieee.org/document/7030390

46. https://pubs.rsc.org/en/content/articlehtml/2022/sd/d1sd00030f
47. Chang J., Wang X., Wang J., Li H., Li F. (2019). Nucleic acid-functionalized metal organic framework-based homogeneous electrochemical biosensor for simultaneous.
48. Zhang X., Yu Y., Shen J., Qi W., Wang H. (2020). Design of organic/inorganic nanocomposites for ultrasensitive electrochemical detection of a cancer biomarker protein. Talanta .2020
49. John D Joannopoulos, Steven G Johnson, Joshua N Winn, and Robert D Meade. Photonic Crystals. In Photonic Crystals. Princeton University Press, 2011.
50. S. K. Yee, Numerical solution of initial boundary value problems involving Maxwell's equations in isotropic media, IEEE Trans. Antennas and Propagation, Vol. 14, pp 302-307, (1966).
51. RSoft Design Group, Inc, BandSolve 4.1 User Guide, license 16847214, 1999-2008.
52. Goyal, A.K., Duttaa, H.S., Pal, S. (2017). Recent advances and progress in photonic crystal based gas sensors. Journal of Physics D: Applied Physics, 50(20). https://doi.org/10.1088/1361-6463/aa68d3
53. Paerhatijiang Tuersun et al ,"Refractive index sensitivity analysis of gold nanoparticles", Vol: 149,pp: 384-390, Optik, 2017.
54. https://www.punarjanayurveda.com/brain-cancer/
55. J. Ferlay, M. Ervik, F. Lam, M. Colombet, L. Mery, and M. Piñeros, Global Cancer Observatory: Cancer Today, https://gco.iarc.fr/today.
56. https://www.ncbi.nlm.nih.gov/books/NBK562165/
57. Udaka YT, Packer RJ (Aug 2018) "Pediatric brain tumors". Neurol Clin 36:533–556. DOI:10.1007/s11060-020-03437-4
58. https://www.advocatehealth.com/health-services/brain-spine-institute/brain-spine-tumors/glioblastoma
59. Ostrom QT, Gittleman H, Fulop J, Liu M, Blanda R, Kromer C, etal., "CBTRUS statistical report: primary brain and central nervous system tumors diagnosed in the United States in 2008–2012," Neuro.Oncol., vol. 17 Suppl 4, pp. iv1-iv62, Oct 2015.DOI: 10.1093/neuonc/not151
60. https://www.lls.org/central-nervous-system-cns-lymphoma
61. https://www.researchgate.net/figure/Preoperative-MRI-demonstrating-vertebral-artery-V4-segment-encased-in-tumor-MRI_fig1_336587349?fbclid
62. https://middlesexhealth.org/learning-center/diseases-and-conditions/brain-metastase

63. https://www.sciencedirect.com/science/article/abs/pii/S0030401816308811?via%3Dihub
64. https://microsoftstart.msn.com/en-us/health/ask-professionals/in-expert-answers-on-braintumor/inbraintumor?questionid=7c3m1m45&type=condition&source=bingmainline_conditionqna
65. Nazmi A. Mohammed, Omar E. Khedr, El-Sayed M. El-Rabaie ,Ashraf A.M. Khalaf, "Brain tumors biomedical sensor with high-quality factor and ultra-compact size based on nanocavity 2D photonic crystal", Alexandria Engineering Journal (2023) 64, 527–540.
66. Biswas, T.; Luu, T. In vivo MR Measurement of Refractive Index, Relative Water Content and T2 Relaxation time of Various Brain lesions With Clinical Application to Discriminate Brain Lesions. Internet J. Radiol. 2009, 13, 1–9
67. Barstugan, Mucahid, Umut Ozkaya, and Saban Ozturk. "Coronavirus (covid-19) classification using ct images by machine learning methods." arXiv preprint arXiv:2003.09424 (2020).
68. Jia, Lin, et al. "Prediction and analysis of Coronavirus Disease 2019." arXiv preprint 2003.05447 (2020).
69. Wang, Bo-Tao, and Qi Wang. "An interferometric optical fiber biosensor with high sensitivity for IgG/anti-IgG immunosensing." Optics Communications 426 (2018): 388-394
70. Magar, Rishikesh, Prakarsh Yadav, and Amir Barati Farimani. "Potential neutralizing antibodies discovered for novel corona virus using machine learning." arXiv preprint arXiv:2003.08447 (2020)

Annex

FDTD method:

The Finite-Difference Time-Domain (FDTD) method is a powerful computational technique used to solve Maxwell's equations numerically for electromagnetic wave propagation problems. It was proposed by Kane S. Yee in 1966 in his seminal paper titled "Numerical Solution of Initial Boundary Value Problems Involving Maxwell's Equations in Isotropic Media."

The FDTD method is based on discretizing Maxwell's curl equations in both time and space domains using finite-difference approximations. The spatial discretization is achieved by representing the computational domain as a grid of Cartesian cells, where the electric and magnetic field components are staggered in space and time, a scheme known as the Yee lattice.

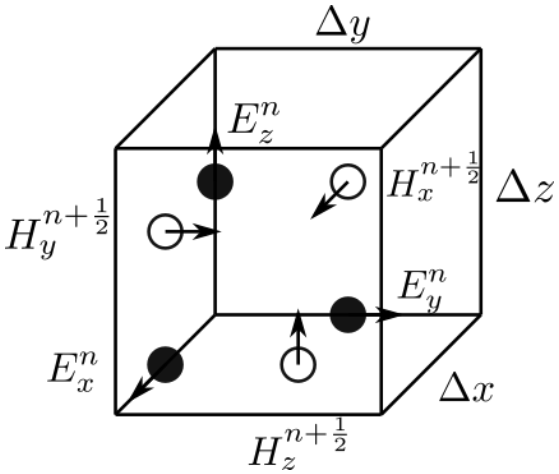

Figure: FDTD method

The key features and steps of the FDTD method are as follows:

1. Yee's Space Lattice: The electric and magnetic field components are arranged in a leapfrog manner on a staggered grid, where the electric field components are positioned at the edges of the cells, and the magnetic field components are positioned at the faces of the cells.
2. Time-Stepping: The FDTD algorithm uses a time-stepping approach, where the electric and magnetic field components are updated alternatively in time using the finite-difference approximations of Maxwell's curl equations.

3. Finite-Difference Approximations: The spatial and temporal derivatives in Maxwell's equations are approximated using central finite-difference approximations, which provide second-order accuracy.
4. Boundary Conditions: Appropriate boundary conditions, such as Perfect Electric Conductor (PEC), Perfect Magnetic Conductor (PMC), or Absorbing Boundary Conditions (ABCs), are applied at the boundaries of the computational domain to model the desired electromagnetic environment.
5. Source Excitation: A source excitation, such as a plane wave or a localized source, is introduced into the computational domain to initiate the electromagnetic wave propagation.
6. Time-Marching: The FDTD algorithm iteratively updates the electric and magnetic field components in a leapfrog manner, advancing in time until a steady-state or a specified time limit is reached.
7. Post-Processing: Once the time-marching is complete, the field components can be used to calculate various electromagnetic quantities of interest, such as radar cross-section, antenna radiation patterns, or electromagnetic field distributions.

The FDTD method has several advantages, including its ability to handle complex geometries, inhomogeneous materials, and dispersive media. It is widely used in various applications, such as antenna design, electromagnetic compatibility analysis, biomedical imaging, and electromagnetic wave propagation studies.

However, the FDTD method also has some limitations, such as the need for a relatively fine discretization to accurately model fine geometrical features or high-frequency problems, which can lead to large computational resources and long simulation times. Additionally, the stair-casing error, which arises from the approximation of curved geometries by a stepped grid, can introduce inaccuracies in certain cases.

Overall, the FDTD method introduced by Yee has become a cornerstone of computational electromagnetics and has been extensively studied, refined, and applied in various fields of electromagnetics and related areas.

Design and Analysis of High Performance 2D Photonic Crystal Based Sensors for Biomedical Sensing Applications

Abstract:

Nowadays, the research on the design and development of wearable label-free biosensors with their potential in human health monitoring has experienced a very rapid growth because of the need to develop high-performing methods to detect and measure low concentrations of specific molecules in various fields. Among all the methods proposed, photonic crystals (PhCs) structures are on focus and offers a good alternative due to their high sensitivity, biocompatibility traits, the capability to control and manipulate the flow of light and enhance field-matter interaction, and the ability to integrate with other electrical components easily. Much attention has been drawn to PhCs biosensors to detect the analyte because of their inherent compactness, high sensitivity, high selectivity, and low cost. In this master's thesis, a novel photonic crystal biosensor based on a two-dimensional photonic crystal (2D-PhC), geared towards rapid biomedical diagnostics at the point-of-care, is proposed and simulated based on refractive index changes of the analyte. The proposed design is simulated using Plane Wave Expansion (PWE) method and Finite-Difference Time-Domain (FDTD) algorithm. The high performance and simple design of the proposed biosensor make it a suitable candidate for bio-sensing applications.

In this context, the work of this master's thesis will consist in studying the sensing performance and evaluating the potentialities of biosensors based on photonic crystals using the RSoft-CAD software.

Keywords: PhC Biosensor, Sensitivity, Q-Factor, Refractive Index, RSoft-CAD, FDTD.

أجهزة الاستشعار القائمة على الكريستال الضوئية المستندة إلى أجهزة الاستشعار لأغراض تطبيقات الاستشعار البيولوجي

ملخص

وفي الوقت الحاضر، شهدت البحوث المتعلقة بتصميم وتطوير أجهزة استشعار أحيائية قابلة للقباس، بما تنطوي عليه من إمكانات في رصد صحة الإنسان، نمواً سريعاً جداً بسبب الحاجة إلى استحداث أساليب عالية الأداء لكشف وقياس التركيزات المنخفضة من جزيئات محددة في مختلف الميادين. ومن بين جميع الأساليب المقترحة، يجري التركيز على هياكل البلورات الضوئية وتوفر بديلاً جيداً نظراً لحساسيتها العالية، وخصائص التوافق الأحيائي، والقدرة على التحكم في تدفق الضوء والتلاعب به وتعزيز التفاعل الميداني-الموضوعي، والقدرة على الاندماج مع المكونات الكهربائية الأخرى بسهولة. وقد وُجِّه الكثير من الانتباه إلى أجهزة الاستشعار الأحيائي التابعة للبلدان التي تمر اقتصاداتها بمرحلة انتقالية للكشف عن التحليل بسبب تشابكها الأصيل، وحساسيتها العالية، وانتقائها العالي، وانخفاض تكلفتها. في أطروحات هذا السيد، يقترح جهاز استشعار أحيائي بلوري ضوئي ضوئي يقوم على بلورة ضوئية ضوئية ثنائية الأبعاد (2D-PhC)، موجهة نحو التشخيصات الطبية الحيوية السريعة في نقطة الرعاية، ويُحاكي استناداً إلى التغيرات في مؤشر الانحلال الانكساري. ويُحتذى التصميم المقترح باستخدام أسلوب الموجة الطائرة التوسّع (PWE) وخوارزمية المجال الزمني (FDTD). ويؤدي الأداء العالي والتصميم البسيط للمستشعر البيولوجي المقترح إلى جعله مرشحاً مناسباً لتطبيقات الاستشعار الأحيائي.

وفي هذا السياق، سيتألف عمل أطروحة الماجستير هذه من دراسة أداء الاستشعار وتقييم إمكانيات أجهزة الاستشعار الأحيائي القائمة على بلورات ضوئية باستخدام برامجيات RSoft-CAD.

الكلمات الرئيسية: مستشعر أحيائي، حساس، Q-Factor، مؤشر تراجع، RSoft-CAD، FDTD.